Improving Urban Cooling in the Semi-arid Phoenix Metropolis: Land System Science, Landscape Ecology and Urban Climatology Approaches

by

Yujia Zhang

A Dissertation Presented in Partial Fulfillment
of the Requirements for the Degree
Doctor of Philosophy

Approved July 2018 by the
Graduate Supervisory Committee:

B. L. Turner II, Chair
Alan T. Murray
Soe W. Myint
Ariane Middel

ARIZONA STATE UNIVERSITY

August 2018

ABSTRACT

The global increase in urbanization has raised questions about urban sustainability to which multiple research communities have entered. Those communities addressing interest in the urban heat island (UHI) effect and extreme temperatures include land system science, urban/landscape ecology, and urban climatology. General investigations of UHI have focused primarily on land surface and canopy layer air temperatures. The surface temperature is of prime importance to UHI studies because of its central rule in the surface energy balance, direct effects on air temperature, and outdoor thermal comfort. Focusing on the diurnal surface temperature variations in Phoenix, Arizona, especially on the cool (green space) island effect and the surface heat island effect, the dissertation develops three research papers that improve the integration among the abovementioned sub-fields. Specifically, these papers involve: (1) the quantification and modeling of the diurnal cooling benefits of green space; (2) the optimization of green space locations to reduce the surface heat island effect in daytime and nighttime; and, (3) an evaluation of the effects of vertical urban forms on land surface temperature using Google Street View. These works demonstrate that the pattern of new green spaces in central Phoenix could be optimized such that 96% of the maximum daytime and nighttime cooling benefits would be achieved, and that Google Street View data offers an alternative to other data, providing the vertical dimensions of land-cover for addressing surface temperature impacts, increasing the model accuracy over the use of horizontal land-cover data alone. Taken together, the dissertation points the way towards the integration of research directions to better understand the consequences of detailed land conditions on

temperatures in urban areas, providing insights for urban designs to alleviate these extremes.

DEDICATION

Dedicated to my parents - Yanling Zhai and Youzhen Zhang

ACKNOWLEDGMENTS

First and for most, I thank my advisor, Dr. B.L. Turner II, for his steadfast support throughout my doctoral studies and providing me with the opportunities to collaborate with a wide variety of gifted scholars. His direction broadened the scope of my research and helped me identify intriguing questions regarding the many challenges faced by urban areas. In addition, my research would have been impossible without the intellectual support of Dr. Alan Murray and his invaluable guidance with regard to spatial science, research design, and professional development. Thanks to Dr. Soe Myint for his insight into remote sensing and urban heat island studies. I thank Dr. Ariane Middel for helping me connect my research with urban climatology and for exposing me to new topics that I otherwise would not have gotten to explore. I am very lucky to have had such an amazing committee that kept me moving forward throughout every stage of this journey.

I express my gratitude towards Drs. Jingle Wu, Kevin McHugh, Anthony Brazel, and Kelli Larson for the substantial influence that their courses have had on my research. Special thanks to Dr. Wei Li for her warm support during my time at ASU. Thanks to my close friends Xiaoxiao Li, Jordan Smith, and Michelle Stuhlmacher, for their enthusiastic encouragement and their assistance in improving my research and writing. Thanks to Rebecca Renee, Zaellotius Wilson, and Alvin Huff for their dedicated assistance during my graduate study. Additional thanks go to Yin Liu, Wan Yu, Chao Fan, Xin Feng, Xiran Zhou, Qunshan Zhao, Wei Kang, Hu Shao, and many others at ASU and beyond.

I would like to recognize my parents for their endless love and for encouraging me to pursue doctoral study. And last but not least, my heartfelt thanks to my husband,

Puyang Li, who has always been supportive of my ideas and plans and has helped me overcome many challenges. I could not have done this without my family.

This dissertation was supported by the Gilbert F. White Fellowship, the Graduate School Completion Fellowship, the Central Arizona-Phoenix Long-Term Ecological Research program (NSF Grant No. BCS-1026865), the Decision Center for a Desert City (NSF Grant No. SES-0951366), the National Science Foundation (NSF) under Grant No. SES-0951366, NSF DMS Grant No. 1419593 and USDA NIFA Grant No. 2015-67003-23508, the Julie Ann Wrigley Global Institute of Sustainability, and the Environmental Remote Sensing and Geoinformatics Lab at Arizona State University.

TABLE OF CONTENTS

Page

CHAPTER Page

CHAPTER Page

LIST OF TABLES

LIST OF FIGURES

CHAPTER 1

URBAN LAND FORMS AND THE URBAN HEAT ISLAND: EXPLORING RESEARCH FIELDS

1.1 Background and Literature Review

The global increase in urbanization has raised questions of urban sustainability (Grimm, 2008; Seto et al., 2017). As a result, various research communities have extended their research interest to problems of the urban heat island (UHI) effect and extreme temperatures. These include overlapping research by land system science, ecology-landscape ecology, landscape architecture, urban climatology, and geo-design (e.g., Flaxman, 2010; Forman, 2016; Grimm, 2008; Sailor, 2001; Seto & Reenberg 2014; Turner, 2017). As cities grow, changes in urban land-covers and their configuration (various labeled urban geometry or morphology, or land architecture), coupled with intensifying human activities, have led to a modified thermal climate, particularly at night, forming a UHI (Fan & Sailor, 2005; Voogt & Oke, 2003). This effect has major consequences for urban sustainability, especially in warm-dry climates, including impacts on energy and water consumption, emissions of air pollutants and greenhouse gases, human health, and the emergence of regional heat islands (Arnfield, 2003; Georgescu et al., 2014; Hondula et al., 2012, 2014; Huang, Zhou, & Cadenasso, 2011; Sailor, 2001). With distinctions in their origins, the noted research communities share overlapping interests and linked approaches in investigating the UHI issue. Urban climate research focuses on surface energy balance and has a strong emphasis on three-dimensional (3D) urban forms (Krayenhoff & Voogt, 2016; Oke, 1988; Oke et al., 2017). The thermodynamic process investigated in urban climatology is one of many processes

operating within the urban system that connects human activities with the surface-atmosphere interactions and the hydrological cycle (Grimm, 2008). Land system science (Turner, 2017) and landscape ecology/urban ecology (Forman, 2016; Wu, 2013) account for largest array land-covers, add their shape to assessments of configuration (but not the vertical dimension), and with geo-design (Flaxman, 2010), employ methods developed in the spatial sciences.

The envelope of air modified by the presence of an urban area is defined as the urban boundary layer in climatology. It can be 1 - 2 km in depth by midday but shrinks to a few hundred meters at night. The majority of the urban boundary layer is assumed to be horizontally homogenous due to turbulence mixing and can be simplified as 1D vertically. The lowest part of the boundary is the urban canopy layer, which rises to 1.5 to 3 times that of the building height. The urban canopy layer exhibits both horizontal and vertical variations and is where the effects of the city are most profound. Consequently, investigations of UHI mostly focused on surface temperature and canopy layer air temperature, which are closely related (Oke et al., 2017, p.31 - 43).

Temperature variations within the canopy layer are caused by the spatial heterogeneity of urban composition and form. To standardize the measuring and modeling of urban composition-form and temperature variations, urban climatology employs a local climate zone classification. Local climate zones are areas of uniform surface cover, structures, material, and human activity that span hundreds of meters to several kilometers in horizontal scale (Stewart & Oke, 2012). It is based on a land-cover classification (dense or scattered trees, low plants, bare soil/sand, paved, water), thermal prosperities (e.g., albedo, emissivity), height and spatial arrangement of building blocks

(low/mid/high; open/compact), and vertical complexity (sky-view factor) that are directly related to the radiation exchange and heat fluxes. This classification scheme creates a continuum of urban form changes from natural to densely developed landscape.

The classification of local climate zones heavily relies on GIS and remote sensing inputs, and there is a growing interest in integrating the abovementioned subfields to investigate the temperature variations within and among local climate zones (Bechtel et al., 2015; Stewart, Oke, & Krayenhoff, 2014). Urban climate research primarily takes a process-based approach, starting from the surface energy balance, examining the mechanisms behind the temperatures variations and ties it with the urban form, thermal propriety, wind dynamics, and sensible/latent heat flux. The thermodynamic process can be modeled using computational fluid dynamic numerical or physical models. Due to the computational complexity, however, the spatial extent of urban climate research is often limited and the interactions among various local climate zones are underplayed (Oke et al, 2017, p.60 - 76; Erell et al., 2012). In contrast, supported by collection of remote sensing inputs, land system science, landscape ecology, and urban ecology focus on large-extent fine-grain composition and pattern analysis. These research communities have explored the importance of an array of land-cover composition (more expansive in kind than that in urban climatology) and their shape, pattern and connectivity (configuration) for temperature variations (Buyantuyev & Wu, 2010; Li, Li, Middel, Harlan, & Brazel, 2016; Myint, Wentz, Brazel, & Quattrochi, 2013; Myint et al., 2015; Lin et al., 2015; Zhou et al., 2011). Configuration analyses are rooted in spatial science, involving the detection and modeling of spatial dependence and heterogeneity, distance-based measures of connectivity and proximity, and geometry measures of compactness and fragmentation,

among other dimensions (Anselin, 1995; Dale & Fortin, 2002; Legendre & Fortin, 1989; Murray, 2010). Their strong emphasis on spatial pattern has complemented the buildings and street canyon dominated studies in urban climatology. This research, however, is largely focused on correlation analysis and tends to lack a process approach anchored in urban climatology.

In contrast to these research fields, geo-design has only recently begun to address questions of the UHI (Flaxman, 2010; Wong et al., 2011). Geo-design uses GIS as the platform to bridge geographic analysis into the design and planning process. Compared to land system science and ecology, geo-design focuses on developing practical tools for urban planners to assess micro-climate conditions, such as the air temperature, solar radiation, ventilation, wind path, and air quality (Jusuf et al., 2012; Wong et al., 2011). Specific web-based tools of collaborative geo-design are still involving, starting from climate data integration to 3D modeling simulation, to real-time GIS simulation platform (Flaxman, 2010).

The various methods of analyses and understanding derived from these fields of research are integrated into this dissertation, with special attention to the use of optimization modeling derived from the spatial sciences. They are applied to the investigation of the surface urban heat island and cool island in the semi-arid metropolis of Phoenix, Arizona.

1.2 Study Area

The Phoenix metropolitan area, one of fastest growing urban regions in the United States, is located on the northern edge of the Sonoran Desert. With a population approaching 1.5 million, the City of Phoenix comprises approximately 1,340 km^2 in the

center of a much larger metropolitan area approaching five million inhabitants and covering 23,494 km^2 (Fig. 1). Dominated by a semi-arid desert climate, the region has low annual rainfall and low relative humidity. Daytime temperatures are high throughout the summer. The winters are mild. May and June are characterized by hot, dry weather. A monsoon season of sporadic but intense rainfall lasts from July to September, whereas winters experience modest frontal precipitation.

Due to extensive urban sprawl, the most abundant urban forms in the metropolitan area are the open low-rise and mid-rise structures, featured by low building height and density, and wide streets, creating a high sky-view factor (Middel et al., 2015; Lukasczyk et al., 2018). Synoptic macroclimate, topography, and urban forms have contributed to the development of strong and stable UHI during the last 50 years. The mean daily air temperature has increased by 3.1 °C and the nighttime minimum temperature by 5 °C (Brazel et al., 2000). The city and metropolitan area confront major UHI effects and related water withdrawal problems, which are expected to be amplified by climate change over the coming years (Gober et al., 2009). Summers in Phoenix are characterized by peaks in energy use and increased residential water consumption (Wentz et al., 2016). High temperatures also increase the potential for heat stress, especially among vulnerable populations. (Chuang & Gober, 2015; Harlan et al., 2006).

The Phoenix UHI has been the focus of many research studies and is closely linked to a policy focused on sustainable urban design (City of Phoenix, 2008, 2010). Existing studies between the land-cover composition and LST have identified the distinction between trees and grasses on LST (Myint et al., 2010). They also concluded that building blocks surrounded by dark impervious surface exacerbate LST. Compact

commercial buildings with high albedo roofs actually reduce daytime LST (Buyantuyev & Wu, 2010; Myint et al., 2010). Beyond the land-cover composition assessments, Li and colleagues (2016), using a novel compactness index, the normalized moment of inertia, demonstrated that land configuration has a stronger influence on LST than land composition at the census block level. This work highlights the importance of attention to shape measures in configuration evaluations and the exploration of spatial methods and metrics other than those from the commonly used FRAGSTAT array generated in ecology (Li, Goodchild & Church, 2013; McGarigal & Marks, 1995). This exploration includes the use of Moran's I by Myint and associates (2015) to examine the effect of spatial configuration on LST, research suggesting that clustered paved surfaces lead to aggregated warming effects.

The above studies use a variety of land-cover spatial scales but LSTs are invariably based on 90 m or coarser data source, largely from ASTER and Landsat. Since surface temperature heterogeneity is scale-dependent, finer scale LST data (< 10 m) better quantifies the surface-UHI pattern and is more valuable for micro-climate modeling and outdoor thermal comfort evaluation. Using the 7 m airborne LST data from MASTER, Jenerette and colleagues (2015) detected positive vegetation-LST relationship and negative building-LST relationship at night, in contrast with the 90 m LST results, indicating that at micro-level, vegetation traps heat and building roofs more rapidly lose heat at night. The study also found that heat-related illness was correlated with parcel-scale daytime LST. Using the same data, Li and associates (2017) concluded that at the parcel level, large land-cover patches of irregular shape improve daytime cooling, while, compact and concentrated land-covers, foremost vegetation, improve nighttime cooling.

In complement to the conventional horizontal land-cover studies, assessment and simulation of the 3D urban form has also been implemented in Phoenix mostly using the micro-climate models, especially in relation to vegetation landscaping and the local climate zone scheme (LCZ) (Chow & Brazel, 2012; Middel et al., 2014; Middel et al., 2015; Zhao, Sailor, & Wentz, 2018). Middel and colleagues (2014) simulated mid-afternoon air and surface temperature distribution, as well as the ventilation and shading conditions of the typical LCZ and landscaping style combinations in Phoenix. Their results demonstrated that mesic landscaping, which has shade trees and expansive turf grass, were the coolest across all the LCZs, followed in order by oasis (dense tree cover) and xeric (sparse trees and no grass) "yardscapes". Widespread use of water-intensive landscapes, which includes turf grass, is contradictory to the long-term sustainability of the metropolitan area. Consequently, the trade-offs should to be considered between extreme temperatures and other dimensions of the environment and resources.

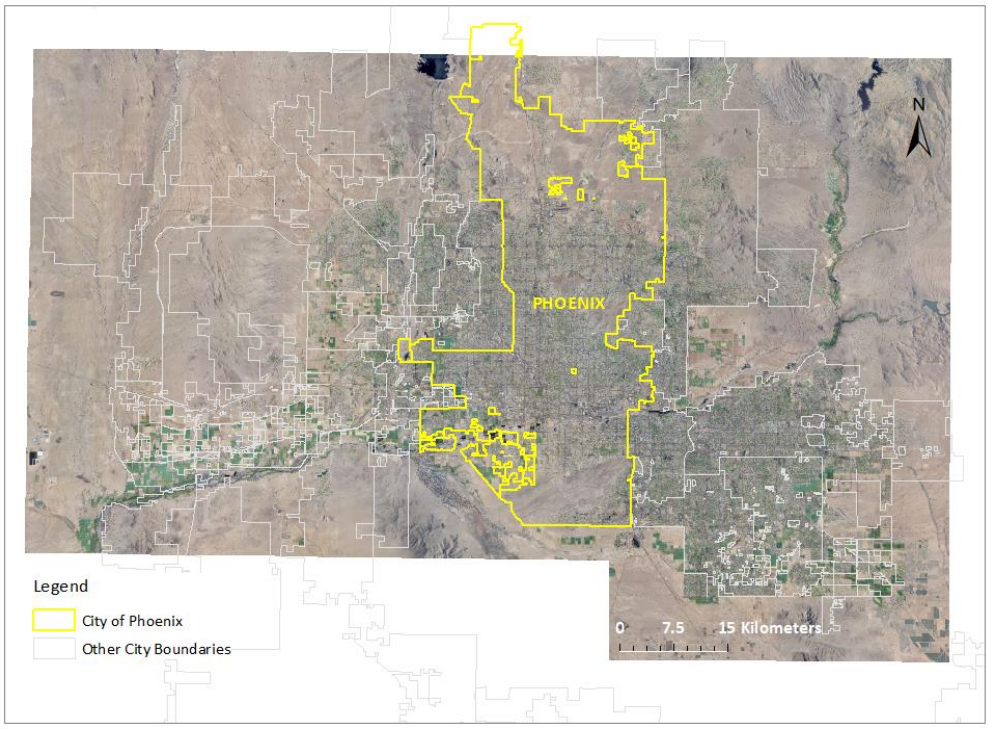

Figure 1. *Metropolitan Phoenix Study Area*

1.3 Research Objectives

The above findings in Phoenix on land-cover composition, configuration, and 3D urban form draw attention to the emerging needs of urban landscape or form optimization in balancing the trade-offs between urban warming, water consumption, and different environmental services in desert cities. Particularly, among various land-use types, green space functions as cool and humid islands in cities, and the strategic arrangement of green space is critical to urban landscape optimization. To date, however, urban cool islands formed by green spaces have not been fully investigated for the Phoenix metropolis.

Focusing on the cool island and the surface heat island effect in Phoenix, Arizona, especially on the diurnal surface temperature variations, this dissertation integrates approaches from land system science, landscape ecology, and urban climatology to

explore the optimal designs of the cityscape to mitigate excessive levels of heat. Foremost by incorporating the fine-tuned, land-cover addressed in land system science and landscape ecology to the vertical dimensions of urban form examined in urban climatology. Specifically, Chapter 2 quantifies and models the cooling benefits of green space considering their locations and spatial arrangements. Chapter 3 optimizes the green space locations to reduce the surface heat island effect and evaluates the day-night cooling trade-offs. Given the limitation of the bird's-eye view, two-dimensional landscape measurements, Chapter 4 links the vertical with the horizontal urban form and evaluates their combined effects on land surface temperature variation. A summary and the significance of the three projects constitute Chapter 5.

CHAPTER 2

QUANTIFICATION AND MODELING OF THE DIRECT AND INDIRECT COOLING BENEFITS OF GREEN SPACE

2.1 Introduction

Green space can effectively reduce temperature through shading and evapotranspiration, relieving urban heat within cities (Oke et al., 2017). Derived from remotely sensed thermal infrared imagery, land surface temperature (LST) shows significant correlation with air temperature and has become an important data source for "park cool island" research (Chang et al., 2007; Lin et al., 2015). Existing studies have shown that the configuration (i.e., size, shape, and pattern) of land-covers, including green spaces, strongly affect temperatures and often exhibit diurnal variation (Myint et al., 2013; Buyantuyev & Wu, 2010). The temperature at any point below the canopy layer, however, is controlled by the unique mix of surface properties within a radius of a few hundred meters. Thus, the cooling diffusion of green spaces is strongly affected by its local environment, an observation that has not been fully investigated (Bowler, 2010; Oke et al., 2017, p.34).

Green space's cooling intensity is defined as the temperature differences between the green space and a selected reference site. City center and nearby weather stations are commonly chosen references. Temperature values from far away sites, however, may have little to do with the cooling diffusion of the green space been examined. Compared to measurements from individual sites, the areal mean value of the local environment is a more appropriate reference for "park cool island" evaluation (Unger, 2008). More importantly, because of air movement and heat exchange, green spaces moderate

temperatures both within and beyond its boundaries, effectively cooling down its neighborhood area. Furthermore, the cooling effects of multiple nearby green spaces may interact, enhancing cooling benefits (Ca et al., 1998; Lin et al., 2015; Spronken-Smith & Oke, 1999). To date, little work has addressed the cooling agglomeration among clustered green space. This study utilizes a 1 m land-cover map and 90 m LST data of part of the metropolitan Phoenix region to solve the following questions:

1. What are the magnitudes of the green space's cooling intensities during the day and at night?
2. When an area is adjacent to more than one green spaces, how large is the additional gain in cooling?
3. How do the characteristics of the green space and its local environment affect the cooling benefit?

These questions imply the following hypotheses:

1. The green space cooling benefit can be quantified/separated as direct and indirect, based on the affected area differences.
2. The magnitude of the indirect cooling benefit increases with the number of adjacent green spaces.
3. The two types of cooling benefits are affected by both the green space and its local environment.

2.2 Data

2.2.1 1 m Land-Cover Map and Green Space Boundaries.

A 1 m land-cover map was created using aerial imagery from the National Agricultural Imagery Program (Fig. 2). The data have four bands (RGB and NIR) and

were acquired for summer 2010. The images were classified using the object-based method, implemented using the eConigtion software (Li et al., 2014). The resulting land-cover data layer included 12 land-cover classes with an overall accuracy of 91.9%. For the purposes of this analysis, the 12 land-cover classes were aggregated into six: building, paved surface, soil, tree (including shrub), grass, and water (Zhang, Murray, & Turner, 2017). The resulting 1 m land-cover data avoids the mixed feature problem of low-resolution data. Thus, it effectively depicts small, fragmented patches and enables examination of individual land-cover effect on LST variations.

Green space boundaries in 2010 were acquired from Maricopa County cadastral data. The green spaces in the Metropolitan Phoenix area consist of a large number of small neighborhood parks that have various parentages of vegetation cover, medium to large size golf courses that are mainly green and well irrigated (recycled water). The total area of green space for 2010 was 6,975 ha, with the median size of seven ha. The average percentage of vegetation cover for these spaces was 60.8%. Green spaces are distributed unevenly across the metropolitan area. Low-income, ethnic minority neighborhoods have less and small-sized green spaces, generally with sparse vegetation cover (Harlan et al., 2006). Older, high-income and largely white neighborhoods have more and larger green space with dense vegetation cover, whereas newer, high-income and largely white neighborhoods have variations of xeric or native vegetation cover.

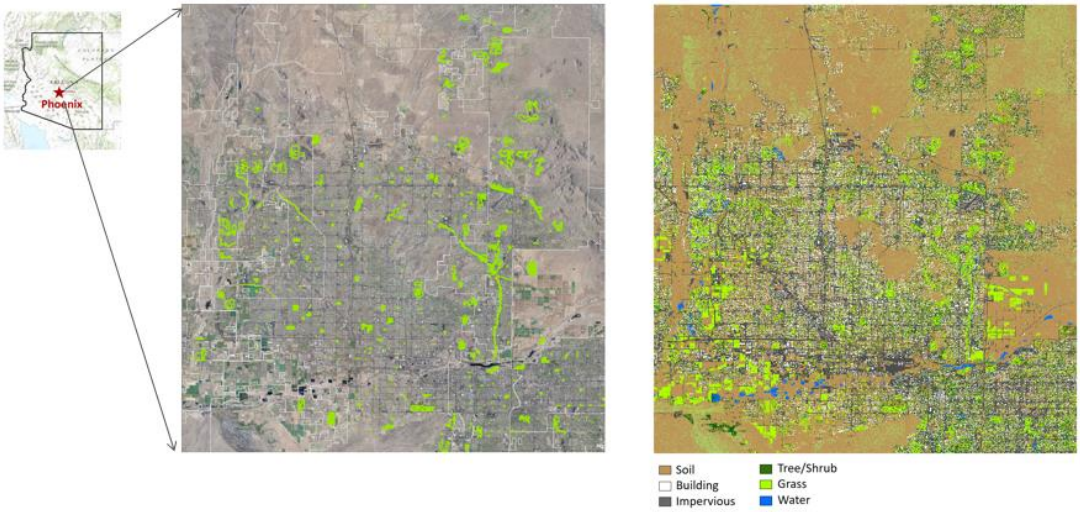

Figure 2. *Green Space Distribution and 1-m Land-Cover Map*

2.2.2 Land Surface Temperature.

LST was derived from Advanced Spaceborne Thermal Emission and Reflection Radiometer (ASTER) data layers (Fig. 3). The ASTER image consists of six bands for short-wave infrared, at 30 m resolution, and five bands of thermal infrared, at 90 m resolution (Yamaguchi et al., 1998). Its multiple thermal wavelength channels facilitate surface emissivity estimation using multispectral methods. The surface temperature measurements were derived from the ASTER_08 product. These data contain surface readings in Kelvin, corrected for atmospheric transmission, emissivity, absorption, and path radiance (Gillespie et al., 1998). The absolute accuracy of the measures ranges from 1 to 4 K, with a relative accuracy of 0.3 K (JPL, 2001). In order to examine the summer diurnal temperature variation, a pair of night and day cloud-free images were selected (under clear and calm weather conditions) in June 17, 2010 (22:00 at local time) and June 18, 2010 (11:00 at local time) (Zhang, Murray, & Turner, 2017).

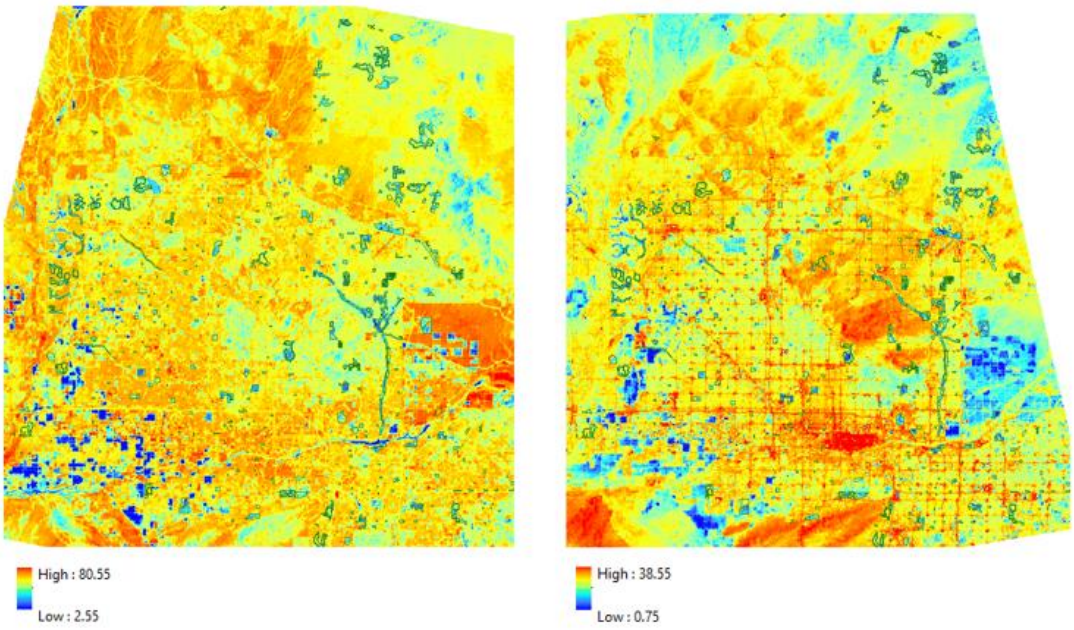

Figure 3. *Day and Night Land Surface Temperature (in °C)*

2.3 Methods

2.3.1 Quantification of the Direct and Indirect Cooling Benefits.

Two types of cooling benefits were quantified mathematically in equations (1) and (2) (Fig. 4). The direct cooling benefits, β, represents the temperature reduction possible if it is green space. It is computed as the mean LST differences between the green space and the local environment. The indirect cooling benefit, δ_k, indicates the temperature reduction possible if there are k nearby green spaces. It is computed as the LST difference between the immediate neighboring area of green space and the local environment.

$$\beta = T - T^* \quad (1)$$

Similarly, indirect cooling benefits can be derived as well:

$$\delta_k = T - T'_k \quad (2)$$

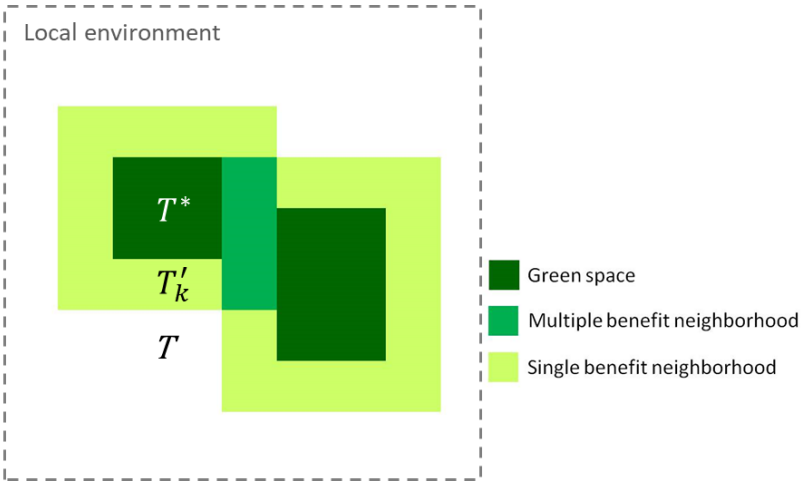

Figure 4. *Conceptual Distribution of Green Space Cooling Benefits*

To identify the proper extent of the neighborhood and the local environment, a series of buffers ranging from 90 to 900 m at 90 m intervals (width of an ASTER image pixel) were created around each green space patch. The appropriate extents were determined based on LST gradient curves of all the green patches. The single and multiple neighborhood areas around each green patch were extracted using GIS intersection and merge methods. Areas that were smaller than 1 ASTER pixel was excluded from subsequent analysis.

2.3.2 Correlation and Regression Analysis of the Direct and Indirect Cooling Benefits.

As noted above, various research indicates that both the composition and configuration of land-cover affect the surface temperature. Based on this research, I selected a narrow set of composition and configuration variables to avoid multi-collinearity among them. The variables are area (TA), percent cover (PLAND), landscape shape index (LSI), and area-weighted mean patch size (AREA_AM). LSI compares the perimeter of a patch to the perimeter of a square of the same size. Higher LSI value

represents a more complex shape. AREA_AM is an adjusted mean patch size measured that weighted larger patches more heavily than smaller patches. Compared to the unweighted version, AREA_AM assumes larger patch has greater ecological importance. The four indicators have simple structures, are easy to interpret, and have been used frequently in various research efforts (Gustafson, 1998; McGarigal et al., 2002). These variables were computed for different land-covers. The large number of predictors were simplified as V_{lmn}, where the subscript *l* indicates the variable type (e.g., area, shape index), *m* indicates the land-cover type (e.g., soil, grass), and *n* indicates the area of aggregation (e.g., green space, neighborhood, local environment).

Moran's I of the cooling benefits was computed to assess the degree of spatial autocorrelation. Pearson correlation analysis was used to assess the associations between the corresponding cooling benefits and V_{lmn}. Multiple linear regression analysis was utilized to estimate the direct and indirect benefits adjacent to one and more than one green space. Forward stepwise and k-fold cross validation methods were adopted to obtain the parsimonious models to avoid multi-collinearity (Hocking, 1976; James et al., 2013).

2.4 Results & Discussion

2.4.1 Quantification of the Direct and Indirect Cooling Benefits.

Based on the LST gradient curves from approximately 500 green space patches, 90 m and 360 m were selected as the extent of the neighborhood and the local environment, respectively. 90 m represents the cooling distance beyond the green space boundary. LST registered by remote sensing instruments is that for the immediate surface observed in the pixel, unaffected by the LST of adjacent pixels. The observation

notwithstanding, cooling distances identified in previous LST based studies range from one to several hundred meters, with large variations by local conditions (Cheng et al., 2014; Lin et al., 2015). Neither study, however, provides a rationale to explain this relationship. Several reasons, all of which apply to the study presented here, follow. The observed temperature-distance observations result from the discrepancy in the sizes of the pixels registering land-cover (1 m) and LST (90 m). In this case, radiations from different ground surfaces are mixed together within the coarser LST pixel (Hu et al., 2015). In addition, tree canopy at the edge of the green space potentially shades and decreases LST outside the green space. Importantly, this study measured LST between and immediately beyond green spaces, identifying the LST relationships. The 360 m local environment extent is consistent with findings from other studies examining the Phoenix area (Fan, Myint, & Zheng, 2015).

Figure 5 displays the percentage of land-cover differences among the three zones. Bar 1 indicates the green space, bar 2 is the neighborhoods, and bar 3 represents the local environment. Among the three zones, green space has distinctive land-cover composition compared to its neighborhoods and the local environment. Land composition of the latter two are quite similar, representing typical residential landscape in Phoenix. Specifically, green space has much higher grass cover (50%) than its neighborhoods and the local environment (10%), and green space's building and impervious percent (5%) are much lower versus the other two (20%). Besides the land-cover composition, Table 1 further compares the means LST differences among the three zones.

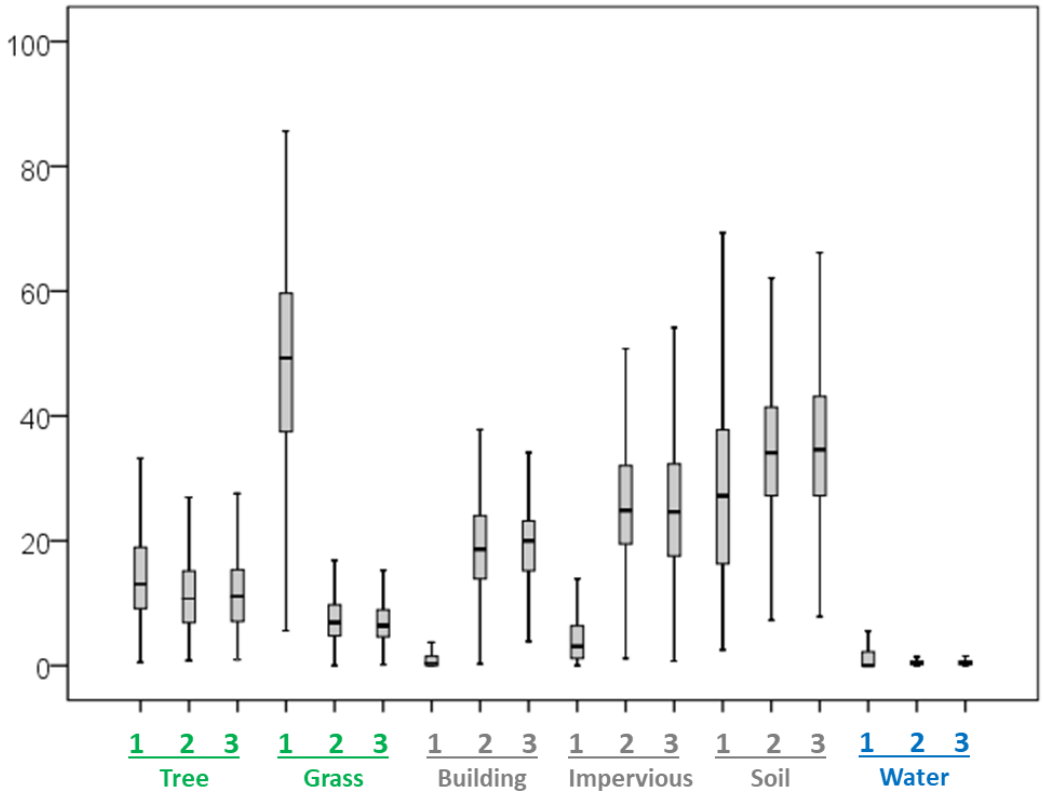

Figure 5. *Percentage of Land-cover Comparisons among the Three Zones*

*1 - green space, 2 - neighborhood, 3 - Local environment

Paired t-test detects significant LST differences across the three zones (Table 1). In specific, the LST differences between the green space and its neighborhood is -2.72 °C during the day and -1.17°C at night. Of particular note are the LST differences between the neighborhood and the local environment. Although they have similar residential landscape, there is still an LST difference of -1.18 °C during the day and -0.47 °C at night between the two. Existing studies commonly compared the LSTs of the green space with its local environment, the neighborhood of the green space, however, has not been investigated yet (Cao et al., 2010; Cheng et al., 2014; Lin et al., 2015). Thus, the above

results support hypothesis 1 that the different types of cooling benefits can be discriminated.

Table 1

Pairwise T-test of Land Surface Temperature Differences

		Paired Differences			**t**	**df**	**Sig.**
		Mean	Std.	Std. Error Mean			
Day	Green space - Neighborhood	-2.72	1.83	0.08	-33.45	512	.000
	Neighborhood - Local environment	-1.18	0.92	0.04	-28.92	512	.000
Night	Green space - Neighborhood	-1.17	0.98	0.04	-26.93	512	.000
	Neighborhood - Local environment	-0.47	0.56	0.02	-19.12	512	.000

Based on Table 1, the direct and indirect cooling benefits (k =1, k >=2) in daytime and nighttime were computed and shown in Figure 6, respectively. The mean value of the direct benefit (β) is 4.17 °C for daytime and 2.33 °C for the nighttime. The values are higher compared to air temperature based studies, which are approximately 1°C during the day and 1.15 °C at night (Bowler et al., 2010; Chang et al., 2007). In terms of the indirect benefit δ_{ik}, during the daytime, when k = 1, the mean value of the δ_{ik} is 2.04 °C. When $k \geq 2$, however, the mean value of δ_{ik} increases to 3.12 °C. During the nighttime, the mean value of δ_{ik} is 1.18 °C (k = 1) and increased to 1.61 °C for $k \geq 2$. The difference of δ_{ik} between the $k \geq 2$ and the $k = 1$ cases indicates the additional cooling gained from neighboring multiple green space. Several studies pointed out the effect of clustered vegetation in decreasing LST, but spatial explicit quantification has not yet been done (Chao, Myint, & Zheng, 2015; Myint et al., 2015). The indirect cooling

differences between the k = 1 and $k \geq 2$ cases support hypothesis 2 that the magnitude of the indirect cooling benefit increases with the number of adjacent green space.

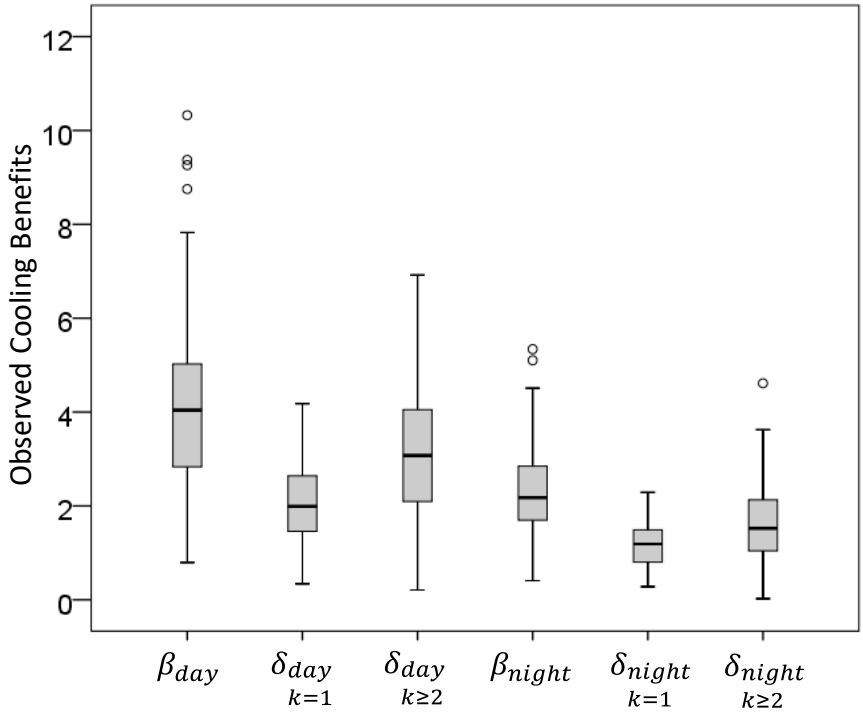

Figure 6. *Direct and Indirect Cooling Benefits*

2.4.2 Correlation and Regression Analysis.

Tables 2 and 3 list the significant land-cover variables, V_{lmn}, in relation to the direct cooling benefit, β. The coefficients of V_{lmn} change greatly in daytime and nighttime, due to the diurnal LST variation (Oke et al., 2017, p. 211). According to table 2, the size and shape of the green space strongly affect β in both daytime and nighttime, which is in line with existing findings. Size primarily controls green space's cooling capacity, but their relationship varied by specific urban landscape, local climate conditions, and quantification differences. Non-linear relationship was reported between size and cooling capacity (Cao et al., 2010; Cheng et al., 2015). In addition, various size

thresholds were identified for effective cooling (Chang et al., 2007; Yu et al., 2018.a; Yu et al., 2018.b).

In terms of the land-cover composition (PLAND) of the green space, grass has the strongest positive association with β in both day and night. Conversely, PLAND of tree is not significant in the day and shows negative effect on cooling at night. This is in line with existing findings that tree and grass function differently in reducing LST, and tree can inhibit nighttime cooling through blocking long-wave radiation from the ground (Erell et al., 2012; Shashua-Bar, Pearlmutter, & Erell, 2009). The PLAND of soil has the strongest negative association with β, followed by the PLAND of building. Compared to the composition variable, the coefficients of configuration variables vary greatly. Previously studies concluded that the effect of land configuration changes depending on the park size, land-cover and image resolution (Zhou et al., 2011; Li et al., 2016; Li, Zhou, & Ouyang, 2013). LSI and AREA_AM of the vegetation and water classes highlight the importance of patch shape and compactness on cooling (Li et al., 2016; Turner et al., 2017).

Fewer variables showed significance within the local environment, and the associations with β are weaker compared to that of the green space. During daytime, composition and configuration of the impervious surface strongly affect β (Table 2). During nighttime, shape complexity becomes a primary factor of β (Table 3).

Table 2

Pearson Correlation Analysis of the Daytime Direct Cooling Benefit

	Landscape	Building	Impervious	Soil	Tree	Grass	Water
Green space							
TA	0.38**						
PLAND		-0.15**		-0.50**		0.45**	0.21**
LSI	0.17**	0.10*	0.18**	0.26**	0.20**	0.17**	0.34**
AREA_AM			0.17**		0.21**	0.55**	0.25**
Local environment							
PLAND			0.13**	0.11*			
LSI		0.16**	0.21**			0.11*	
AREA_AM			0.28**				

*TA - Total area, PLAND - percent of cover, LSI - landscape shape index, AREA_AM - area-weighted mean patch size

Table 3

Pearson Correlation Analysis of the Nighttime Direct Cooling Benefit

	Landscape	Building	Impervious	Soil	Tree	Grass	Water
Green space							
TA	0.51**						
PLAND		-0.12*	-0.11*	-0.33**	-0.12*	0.44**	
LSI	0.28**	0.25**	0.24**	0.34**	0.33**	0.26**	0.34**
AREA_AM			0.13*	0.12*		0.61**	0.19**
Local environment							
PLAND				0.23**			
LSI		0.16*	-0.13*	-0.14*	0.16**	0.20**	0.13*
AREA_AM							

*TA - Total area, PLAND - percent of cover, LSI - landscape shape index, AREA_AM - area-weighted mean patch size

Table 4 lists the daytime regression results of the direct benefit, β_{day}. Overall, 52% of the β_{day} variation was explained by seven predictors, including five green space variables and two local environment variables. The standard error of estimation is

1.44 °C. All of the variables show a positive effect on β_{day}. Among them, PLAND of grass has the strongest impact, followed by the AREA_AM of tree, PLAND of water, and the shape index of soil. Compare to studies that only use predicators of the green space, additional local environment predictors also show significant impact on cooling benefit (Cheng et al., 2015; Cao et al., 2010). In this case, a high proportion of impervious and soil cover outside the green space increase the LST gradient, thus increase β. In addition, the small VIF values indicate a low level of multi-collinearity among the predictors. The residuals have no strong sign of spatial autocorrelation. The nighttime regression results are listed in table 5. R^2 of the β_{night} model is 0.52, with a standard error of estimation of 0.72 °C.

Table 4

Regression Analysis of the Daytime Direct Cooling Benefit

Predictors		**Std. Coef**	**Sig.**	**VIF**
Constant			.00	
Green space	**grass_pland**	0.45	.00	1.55
	tree_area_am	0.29	.00	1.08
	grass_area_am	0.29	.00	1.53
	water_pland	0.18	.00	1.08
	soil_lsi	0.18	.00	1.36
Local	**impervious_pland**	0.32	.00	2.14
environment	**soil_pland**	0.21	.00	2.27
Model Summary				
	R^2	**0.52**		
	Sig.	.00		
	Std. error	1.44 (°C)		

*TA - Total area, PLAND - percent of cover, LSI - landscape shape index, AREA_AM - area-weighted mean patch size

Table 5

Regression Analysis of the Nighttime Direct Cooling Benefit

Predictors		**Std. Coef**	**Sig.**	**VIF**
Constant			.27	
Green space	**landscape_ta**	0.45	.00	2.44
	grass_pland	0.34	.00	1.65
	grass_area_am	0.28	.00	1.90
	tree_area_am	0.10	.02	1.13
Local	**soil_area_am**	-0.18	.00	2.46
environment	**soil_pland**	0.16	.01	2.69
	paved_lsi	-0.11	.03	1.70
Model Summary				
	R^2	**0.52**		
	Sig.	.00		
	Std. error	0.72 (°C)		

*TA - Total area, PLAND - percent of cover, LSI - landscape shape index, AREA_AM - area-weighted mean patch size

Table 6 lists the daytime regression results of the indirect cooling benefit, $\delta_{day,k=1}$. Overall, half of $\delta_{day,k=1}{}'s$ variation is explained by nine variables, including four from the green space, three within the neighborhood, and two within the local environment. The standard error of estimation is 0.72 °C. Seven of the nine predictors belong to tree or grass, reflecting their dominant impact on indirect cooling. According to the standardized coefficients, tree and grass cover within the neighborhood have the strongest positive effect on $\delta_{day,k=1}$; conversely, tree and grass cover of the local environment show the strongest negative effect. Green space variables show relatively weak but significant impact on indirect cooling. The R^2 of the nighttime model is 0.4, with a standard error of 0.37 °C (Table 7). The result demonstrate that indirect cooling in not only affect by land-cover of the neighborhood area, but also closely relates to

landscapes of green space and the local environment. In sum, the above correlation and regression results support hypothesis 3 that the direct and indirect cooling benefits are affected by the land composition and configuration of the green space and its local environment.

Table 6

Regression Analysis of the Daytime Indirect Cooling Benefit (k=1 case)

Predictors		**Std. Coef**	**Sig.**	**VIF**
Constant			.00	
Green space	**soil_pland**	-0.24	.00	2.59
	grass_pland	0.22	.00	2.77
	tree_area_am	0.12	.00	1.24
	grass_area_am	0.09	.04	1.42
Neighborhood	**tree_pland**	0.56	.00	5.10
	grass_pland	0.27	.00	1.87
	build_lsi	0.16	.00	1.35
Local environment	**tree_pland**	-0.64	.00	4.89
	grass_pland	-0.30	.00	1.80
Model Summary				
	R^2	**0.49**		
	Sig.	.00		
	Std. error	0.72 (°C)		

*TA - Total area, PLAND - percent of cover, LSI - landscape shape index, AREA_AM - area-weighted mean patch size

Table 7 Regression Analysis of the Nighttime Indirect Cooling Benefit (k=1 case)

Predictors		**Std. Coef**	**Sig.**	**VIF**
Constant			.00	
Green space	**grass_area_am**	0.27	.00	1.36
	soil_pland	-0.22	.00	1.33
Neighborhood	**paved_lsi**	0.47	.00	2.25
	paved_pland	-0.27	.00	2.69
Local environment	**paved_lsi**	-0.46	.00	2.26
	paved_pland	0.42	.00	2.79
Model Summary				
	R^2	**0.40**		
	Sig.	.00		
	Std. error	0.37 (°C)		

*TA - Total area, PLAND - percent of cover, LSI - landscape shape index, AREA_AM - area-weighted mean patch size

2.5 Limitations

The major limitation in this study is the use of LST to measure distant cooling effects. Unlike air temperature, LST for any unit observed does not mix in principle. Hence, the cooling distance observed away from or between green spaces, has yet to be formally linked, although it is observed in a number of studies (Cheng et al., 2014; Lin et al., 2015). Future examination that compares remote sensing derived LST with in situ LST measures in cities are required to address this issues. In addition, in situ validation results show that the ASTER LST accuracy was generally within ± 1K, with higher accuracy in a drier atmosphere and more homogenous landscape (Hulley, Hughes, & Hook, 2012). The error propagation of LST retrieval on cooling quantification should be further examined.

This study uses the multiple ordinary least squares (OLS) regression, which is commonly used for LST land-cover assessments. Its results are easier to interpret and to

compare across cases. Nevertheless, OLS model has many limitations, existing LST-land-cover models generally achieve an R^2 around 0.5 or less (Connor, Galletti, & Chow, 2013; Li et al., 2016; Myint et al., 2013; Zhou et al., 2011). To address this, spatial regression and non-linear models were adopted to improve parameter estimate and model fit (Li et al., 2012; Chao, Rey, & Myint, 2016; Cheng et al., 2015). More importantly, variables that directly related to surface energy exchange, such as surface albedo, humidity, shading condition, and vertical urban form should also be added to better quantify the underlying thermal process (Voogt & Oke, 2003).

2.6 Conclusions

Using fine-scale land-cover and surface temperature data, this study quantifies both the direct and indirect cooling effects of green spaces and evaluates the degree of cooling increments resulting from clustered green space. Results demonstrated that the average direct benefit is approximately 4 °C during the day and 2 °C at night for green spaces in Phoenix metropolis. Furthermore, the indirect benefit up to 90 m from the green island is about 2 °C during the day and 1.5 °C at night based on surface temperature measurements. Regression results suggest that in addition to size, land-cover type, and shape, green space cooling also depends on the surrounding land-cover context, the number of green spaces in proximity to one another, and the diurnal surface-UHI variations. These findings hold for the summer desert environment of the Phoenix metropolitan area, demonstrating the spatial dependence of the cooling effect that can be used to optimize green space location. The approach employed, however, can be used for green space cooling assessment for other urban areas.

CHAPTER 3

OPTIMIZING THE GREEN SPACE LOCATIONS TO REDUCE THE SURFACE-UHI IN DAY AND NIGHT[1]

3.1 Introduction

As cities grow, changes in urban land-cover and geometry/morphology/architecture coupled with intensifying human activities have led to a modified thermal climate, particularly at night, forming an urban heat island (UHI) (Fan & Sailor, 2005; Voogt & Oke, 2003). This effect has significant implications for sustainability, with consequences for energy and water consumption, emissions of air pollutants and greenhouse gases, human health, and the emergence of regional heat islands (Arnfield, 2003; Hondula et al., 2012, 2014; Huang et al., 2011; Georgescu et al. 2014; Sailor, 2001). The UHI effect is intense in Phoenix, Arizona, amplified by rapid and extensive urbanization with resulting temperature increases approximating 0.5 °C per decade (Grimm et al., 2008). Summers in Phoenix are characterized by peaks in energy use and increased residential water consumption as well as the emergence of extreme UHI "riskscapes" (Harlan et al., 2006; Jenerette et al., 2011; Ruddell et al., 2010; Wentz et al., 2016).

Green space, an area partially or completely covered by grass, trees, shrubs, and/or other vegetation in the form of parks, golf courses, large gardens, and yards, can effectively reduce temperature through shading and evapotranspiration (Balling & Lolk,

[1] This chapter appeared in the following: Zhang, Y., Murray, A. T., & Turner, B. L. (2017). Optimizing green space locations to reduce daytime and nighttime urban heat island effects in Phoenix, Arizona. *Landscape and Urban Planning, 165*, 162-171. To be consistent with this dissertation, several paragraphs in the original paper are omitted and appear in Chapter 2. These omission are noted by footnotes in Chapter 3 designating the reader to the appropriate parts of Chapter 2.

1991; Chang et al., 2007; Spronken-Smith & Oke, 1998). Recognizing the potential to mitigate UHI, the City of Phoenix has launched a master plan that aims to increase the amount of green space (City of Phoenix, 2010). Consequently, an important question is where to site new green space in order to best realize potential cooling benefits. Improvements in measuring and modeling cooling benefits of green spaces are required, however, to make informed decisions.

On the measurement side, air temperature based studies have found that green space can be 1 to 3 °C, and sometimes even 5 to 7 °C, cooler than surrounding built-up areas (Spronken-Smith & Oke, 1998; Upmanis et al., 1998; Chow et al., 2011), with cooling impacts extending as much as several hundred meters beyond green space boundaries (Spronken-Smith et al., 2000; Eliasson & Upmanis, 2000; Bowler et al., 2010). Air temperature measurements are not suitable for citywide studies, however, due to their small sample size and limited spatial coverage (Bowler et al., 2010). Derived from remotely sensed thermal infrared imagery, land surface temperature (LST) measures surface-UHI (SUHI). LST shows significant correlation with air temperature and provides complete spatial coverage across an entire cityscape (Buyantuyev & Wu, 2010; Fung et al., 2009; Klok et al., 2012; Nichol et al., 2009). Extensive research has explored relationships between SUHI and urban land-cover, especially with regard to vegetation (Buyantuyev & Wu, 2010; Li et al., 2016; Myint et al., 2013; Ren et al., 2013; Weng, 2009; Zhou et al., 2011). Studies have suggested that land-cover composition and configuration of the green space are strong predictors of its cooling effect (Cao et al., 2010; Lin et al., 2015; Li et al., 2012; Maimaitiyiming et al., 2014; Ren et al., 2013). Furthermore, local context and adjacent green space also have impacts on cooling (Cheng

et al., 2014; Lin et al., 2015; Spronken-Smith & Oke, 1998, Spronken-Smith & Oke, 1999). Explicit linkages between cooling effects and the locations of green spaces are missing, however, causing difficulties for location model construction.

On the modeling side, micro-climate numerical models deal with surface energy balance, simulating thermodynamic processes for canopy layer UHI assessment (Chow et al., 2011; Erell et al., 2012; Fernández et al., 2015; Middel et al., 2015; Ng et al., 2012). Results from such models are rich in temporal scale but are limited in spatial extent, thus fail to capture intra-urban temperature variations. Combining broader scale spatial data, multi-objective optimization models have been applied recently to determine green space locations in the city, balancing various kinds of environmental benefits. Neema and Ohgai (2013) developed a multi-objective heuristic technique for optimizing the configuration of parks and open space with respect to air and water quality improvement as well as noise and temperature reduction. Zhang and Huang (2014) sought to minimize LST in the allocation of land-uses within a multi-objective heuristic, where temperature is a regressed function of land-use intensities. As yet, however, no current model has attempted to account for the agglomeration of cooling resulting from adjacent green spaces, which greatly affects their spatial allocation.

The above-mentioned measuring and modeling gaps are addressed in this research using an integrated framework that combines remote sensing, GIS, spatial statistics, and spatial optimization. Fine-scale remote sensing data can greatly improve model reality, allowing better representation of the intra-urban SUHI intensities. Incorporated with GIS, statistical and optimization models facilitate practical location decision making to enhance green space cooling. The study first quantifies and predicts direct and indirect

cooling benefits of the green space using LST and land-cover data, linking cooling effect with green space locations. The exact formulation and solution for green space allocation is developed next and explicitly accounts for agglomeration-based cooling. The multi-objective model developed here considers both daytime and nighttime cooling impacts, enabling trade-off solutions to be identified. The framework is applied to an area in central Phoenix.

3.2 Data

Associated data utilized in this study include thermal temperature readings and a fine-scale land-cover classification. The LST was derived from Advanced Spaceborne Thermal Emission and Reflection Radiometer (ASTER) data layers. The ASTER image consists of six bands for short-wave infrared, at 30 m resolution, and five bands of thermal infrared, at 90 m resolution (Yamaguchi et al., 1998). The ASTER_08 product was used for surface temperature extraction. In order to address the diurnal cooling effect variation, a night and day cloud-free image pair were selected (under clear and calm weather conditions) for a summer period: June 17, 2010 (22:00 at local time) and June 18, 2010 (11:00 at local time), respectively. Daytime and nighttime temperatures for these dates at 90 m resolution are shown in Figure 7. The study area consists of 11,466 (126 by 91) pixels. The mean surface temperature of the area is 55.60 °C and 29.85 °C for day and night, respectively. Table 8 shows the comparison between air temperature from weather stations and corresponding LST values. This highlights significant daytime differences between the surface and air temperatures because LST responds to direct solar radiation (Cao et al., 2010; Hartz et al., 2006). During nighttime, the surface temperatures are slightly higher than air temperatures. Calm wind conditions enhance the

positive association between LST and air temperature, whereas strong winds decouple the relationship (Stoll & Brazel, 1992).

Both daytime and nighttime effects are examined because of their combined impacts on human well-being, energy and water use, and environmental performance. The well-known consequences of extreme summer temperatures in the Phoenix area include human health (Harlan et al., 2006), increased demands on energy for cooling and water for landscaping (Wentz et al., 2016), and impacts on year-round tourism favored by the commercial sector (Gober et al., 2009). Perhaps less known are the nighttime UHI effects. These include extending energy use for cooling into the evening, owing to daytime heat storage (Grimmond & Oke, 2009), and throughout the night, as well as providing a higher temperature base from which the daytime UHI effect builds (Stoll & Brazel, 1992). Interestingly, higher nighttime temperatures during the winter reduce the occurrence of frost and its dampening effect on insects and arthropods, which in turn increase pesticide use, among other impacts (Ruddell et al., 2013).

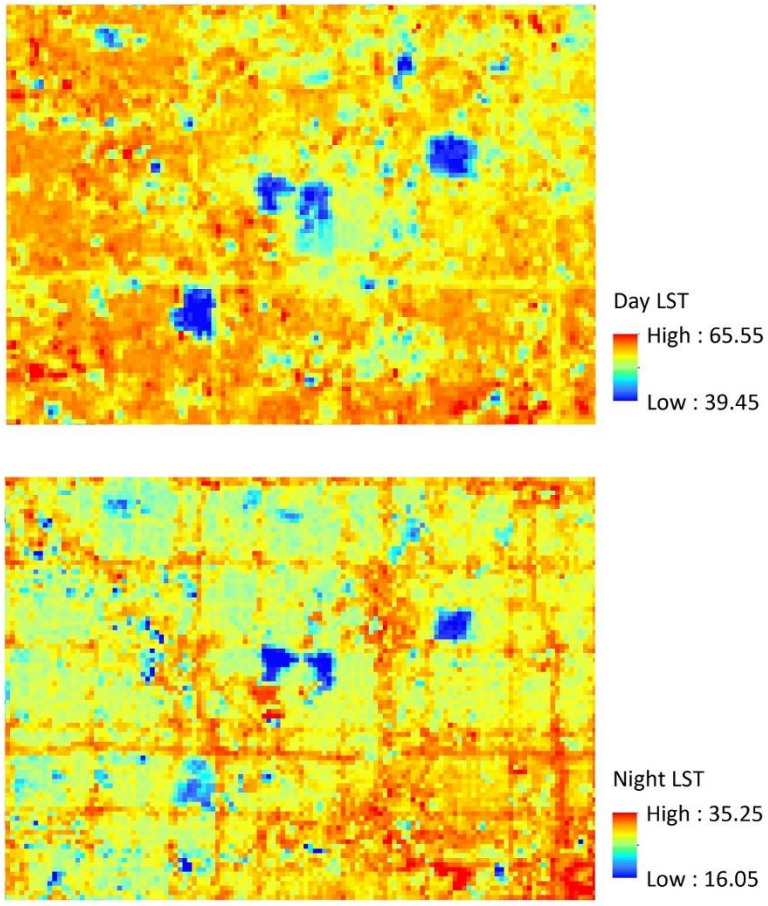

Figure 7. *Observed Day and Night Land Surface Temperature (in °C)*

Table 8

Comparison of Air Temperature and Land Surface Temperature

Weather Stations	Air Temperature (at 11:00)	Land Surface Temperature (at 11:00)	Air Temperature (at 22:00)	Land Surface Temperature (at 22:00)
Mesa	35.00	53.65	30.78	30.95
Phoenix Sky Harbor	35.33	56.75	33.61	31.35
Phoenix Encanto	34.50	44.95	25.72	26.80
Phoenix Greenway	34.00	45.85	27.78	27.35
Desert Ridge	32.39	45.35	25.61	28.15

In addition, a 1 m land-cover classification of metropolitan Phoenix was utilized. This data layer was created using aerial imagery from the National Agricultural Imagery Program. The 1 m aerial images have four bands (RGB and NIR) and were acquired for summer 2010. The images were classified using the object-based method, implemented using the eConigtion software (Li et al., 2014). The resulting land-cover data layer included 12 land-cover classes with an overall accuracy of 91.9%. For the purposes of this analysis, the 12 land-cover classes were aggregated into 6 classes: building, paved surface, soil, tree (including shrub), grass and water (Fig. 8).

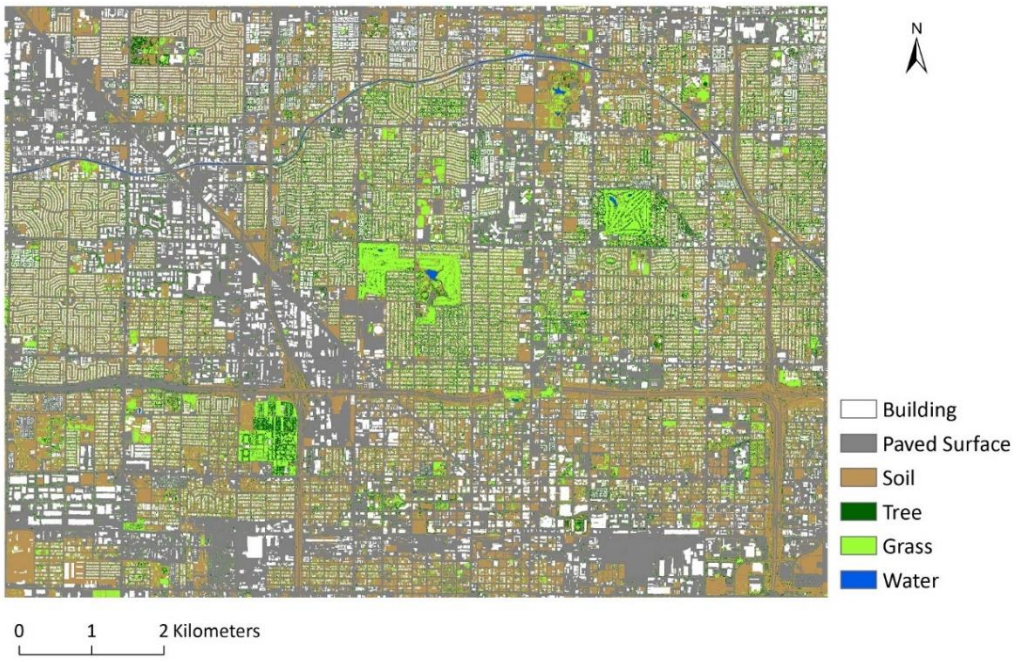

Figure 8. *1 m Land-cover data Map*

3.3 Methods[2]

Green space provides local heat reduction that may contribute to region-wide benefits. Because of air movement and heat exchange, green space moderates temperatures within and beyond its boundaries, effectively forming neighborhood cooling (Ca et al., 1998; Spronken-Smith & Oke, 1998; Spronken-Smith et al., 2000). Furthermore, the cooling effects of nearby green space may interact, enhancing local benefits (Lin et al., 2015; Spronken-Smith & Oke, 1999). A conceptualization of this is illustrated in Chapter 2, Figure 4. For a given area *i* (or cell, parcel or land management zone), given the temperature for an area as it currently exists, T_i. T_i^* indicates the anticipated temperature if it were to be converted to green space, and T'_{ik} denotes the

[2] The direct and indirect cooling benefit quantification are illustrated in Chapter 2, page 15 and Figure 4.

anticipated temperature for area i if exactly k green spaces are neighboring i. In this case, T_i is estimated using the mean temperature of the local surrounding, which reflects the temperature without the cooling effect. Proximity corresponding to neighborhood and the local surrounding extents were quantified in Chapter 2. β_i represents the direct temperature reduction possible if it is green space and δ_{ik} indicates the indirect temperature reduction possible if there are k nearby green spaces.

To address urban heat island challenges, a spatial analytic framework that incorporates remote sensing, GIS, spatial statistics, and spatial optimization (Fig. 9) is proposed. Remote sensing provides essential data inputs, such as land-cover and surface temperature measurements. GIS offers methods for integration and management of spatial information, important spatial analytic functions for deriving β_i and δ_{ik}, capability to structure the optimization model based on data inputs, and support to visualize and evaluate green space planning results. Spatial statistical analysis is used to predict cooling benefits, β_i and δ_{ik}, based on observed temperature, T_i, and land-cover variables within and surrounding an area i. Spatial optimization is used for formalizing and solving the green space planning model. Each component requires data from or contributes data to GIS. Particularly important, however, are derived parameters and spatial information layers that are fed back into GIS.

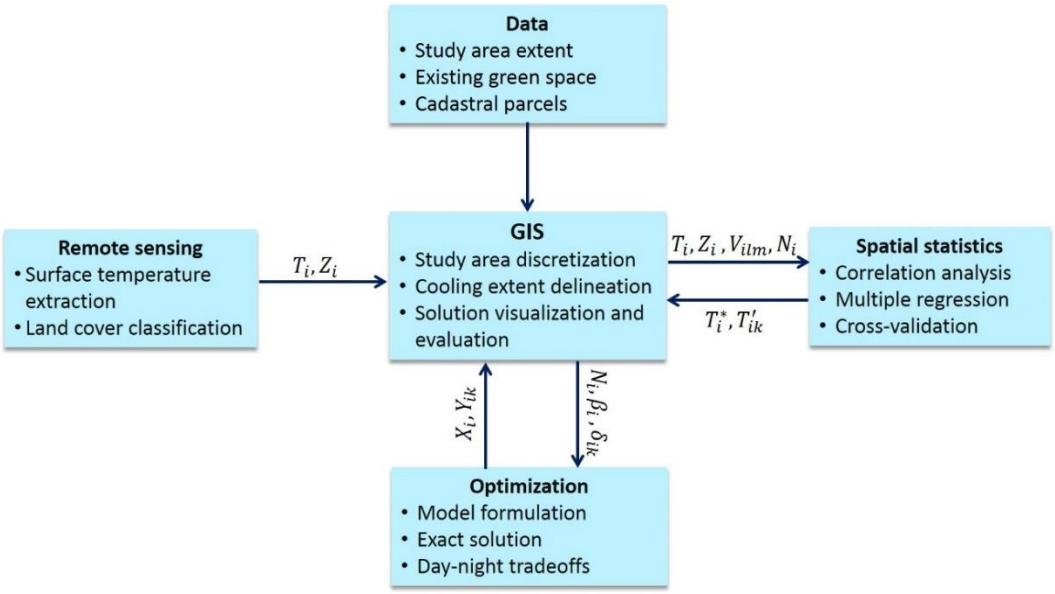

Figure 9. *Methodological Framework*

3.3.1 Remote Sensing.

The thermal imagery supports green space optimization through the extraction of surface temperature across a region. This is far more comprehensive and complete than traditional spatial sampling approaches that rely on ground-based equipment readings combined with interpolation. The surface temperature measurements were derived using ASTER_08 imagery, as noted previously. The data contains surface readings in Kelvin, corrected for atmospheric transmission, emissivity, absorption and path radiance (Gillespie et al., 1999). The absolute accuracy of the measures ranges from 1 to 4 K, with a relative accuracy of 0.3 K (JPL, 2001). The readings were then converted to Celsius. The output is observed LST, T_i, for each of the 11,466 land units (cells) in the study area. The 1 m land-cover data layer was classified using the object-based method based on the four bands aerial imagery, also noted previously. The aerial imagery was first segmented into parcel sized objects using cadastral parcel boundaries. Then, integrating spectral,

contextual, geometrical information and expert knowledge, a hierarchical classification rule set was created to further assign and segment the image objects into detailed land-cover classes (see Li et al., 2014). The result 1 m land-cover map avoids the mixed feature problem of low-resolution data. Thus, it effectively depicts small, fragmented green space and enables examination of individual land-cover effect on cooling (Li et al., 2013; Myint et al., 2013). The output is land-cover, Z_i, for each of the 11,466 land units (cells) in the study area. ERDAS IMAGINE was utilized for all remote sensing processing.

3.3.2 GIS.

GIS is a central component in this framework, connecting remote sensing, spatial statistical and optimization through data management, manipulation, analysis, and visualization. The study area was first discretized into 11,466 land units (cells), with each cell of the size of 0.81 ha. Next, neighbor and local area buffers were delineated for each area i at 90 m and 360 m, respectively, based on observed temperature gradients around green space. Land-cover variables,V_{ilmn}, were also derived using FRAGSTATS, a spatial analytical software for landscape analysis(McGarigal & Marks, 1995)[3]. Another proximity based attribute derived using GIS was adjacency, where neighboring units are in the set N_i for each area i, which is associated with the indirect cooling. This information is utilized in land-cover evaluation, statistical analysis, and optimization. A final aspect of GIS is that results from statistical analysis and spatial optimization are readily displayed for evaluation in various ways. ArcGIS was utilized for all GIS processing.

[3] See detailed descriptions of V_{ilmn} in Chapter 2, page 16.

3.3.3 Statistical Analysis.

As noted previously, research has established that size, shape, and land-cover of green space are strong predictors of its cooling effect. Furthermore, the cooling benefit is location dependent, affected by the surrounding land-cover as well (Cheng et al., 2015). The formal specifications of cooling benefits are given in Chapter 2, equations (1) and (2). Critical of course is the estimated temperatures associated with green space, T_i^* and T'_{ik}, where the former is expected temperature if area i is converted to green space and the latter is the expected temperature when exactly k green spaces are nearby. In general, expected temperature is a function of a variety of observed characteristics for each area (and/or neighboring areas):

$$T_i^* = f(T_i, Z_i, V_{ilmn}, N_i) \quad (3)$$

$$T'_{ik} = g\left(j \in N_i, Z_j, T_j, V_{jlmn}\right) \quad (4)$$

Precise mathematical specification is based on components of the spatial statistical module of the framework involving correlation analysis, multiple linear regression, and cross-validation methods. Model fitness was statistically significant, with no issues of spatial autocorrelation or multicollinearity. More than 300 observed green space areas in Phoenix enabled appropriate parameters to be derived for temperature estimation in both day and night conditions. SPSS and R package were utilized for all statistical analysis.

3.3.4 Optimization.

An optimization model was structured to identify the best locations for new green space in order to realize the greatest overall benefits. The accounts for both the direct and indirect benefits and taken extends the coverage location model of Church and ReVelle (1974) (see also Church & Murray, 2009; Murray et al., 2010) in a number of ways.

Specially, β_i accounts for direct cooling benefits. In addition, δ_{ik} accounts for the indirect cooling enhancement associated with k, where *k* explicitly notes the number of times an area neighbors green space. The notation of the discrete integer optimization model was defined as follows:

j = index of potential green space areas

i = index of areas

k = number of neighboring green spaces

β_j= cooling benefit for converting area j to green space

δ_{ik}=cooling benefit received area i from k neighboring green spaces

N_i = set of areas neighboring unit i

p = number of green spaces to location in a region

$X_j = \begin{cases} 1 \text{ if area } j \text{ converted to green space} \\ 0 \text{ if not} \end{cases}$

$Y_{ik} = \begin{cases} 1 \text{ if area } i \text{ neighbors } k \text{ green spaces} \\ 0 \text{ if not} \end{cases}$

The developed coverage is formulated as follows:

Maximize $\sum_j \beta_j X_j + \sum_i \sum_k \delta_{ik} Y_{ik}$ (5)

Subject to $kY_{ik} - \sum_{j \in N_i} X_j \leq 0 \ \ \forall j, k$ (6)

$\sum_k Y_{ik} + X_i \leq 1 \ \ \forall i$ (7)

$\sum_j X_j = p$ (8)

$X_j = \{0,1\} \ \ \forall j$ (9)

$Y_{ik} = \{0,1\} \ \ \forall i, k$

The objective, (5), is to maximize the total sum of cooling benefits, either directly or indirectly. Constraints (6) define whether the indirect cooling benefit is provided to

area i. Constraints (7) ensure that at most one of the two types of cooling benefits is provided to an area. Constraint (8) specifies that p areas are to be converted to green space. The value of p is predetermined base on the goals associated with the city's plan. Finally, binary restrictions are imposed on decision variables in Constraints (9). To assess the day-night trade off, a weighted multi-objective model can be structured. Assume the following:

$$\Omega_{day} = \sum_j \beta_{day,j} X_{day,j} + \sum_i \sum_k \delta_{day,ik} Y_{day,ik} \quad (10)$$

$$\Omega_{night} = \sum_j \beta_{night,j} X_{night,j} + \sum_i \sum_k \delta_{night,ik} Y_{night,ik} \quad (11)$$

The difference between (10) and (11) are the values of β_j and δ_{ik} depending on whether it is day or night conditions. The two objectives can be integrated using a weighting variable w as follows:

$$\textit{Maximize} \qquad w\Omega_{day} + (1-w)\Omega_{night} \quad (12)$$

where $w \in [0,1]$. Thus, this model can be repeatedly solved for different values of w, with each unique solution representing a valid and potentially meaningful trade-off solution. Planning and decision-making processes would, therefore, take this information into account prior to plan implementation.

The analysis was carried out on an Intel i5 (3.10 GHz) computer running Windows 7 64-bit with 8 GB of RAM. ArcGIS 10.2 was used to discretize the study area and delineate the cooling coverage. Arcpy and Gurobi python API were employed to import the location information and constructed the mixed integer model. The model was then solved in Gurobi using the branch-and-bound approach. The original model contained 2,935,297 rows, 2,935,552 columns and 16,511,232 nonzero elements. The presolve process in Gurobi first tightens the formulation, with a reduced model size of

93,899 rows and 377,020 columns, with 1,120,292 nonzero elements. The linear relaxation is used to establish an upper bound, with feasible integer solutions establishing valid lower bounds. The optimality gap between the upper and lower bound converges to zero within less than three minutes through the use of branch and bound.

The moving window approach will be used to compute the β_j and δ_{ik} at per pixel location (90 m by 90 m) based on regression models developed from Chapter 2 using the 1m land-cover map. Arcpy and Gurobi python API were used employed to import the location information and constructed the mixed integer model. The model was then solved in Gurobi using the branch-and-bound approach.

3.4 Results

3.4.1 The Predicted Cooling Benefits.[4]

Figure 10 summarizes the predicted β_i across the study area, which was the direct cooling benefit for area i if it is converted to green space. The daytime mean value is 6.7 °C. The nighttime mean value is 2.6 °C. We assume the green conversion had identical land-cover, which is 100% grass. Grass cover is selected because of its simpler effects on radiation and surface energy balance compared to trees. Unlike grass, trees affect cooling in positive and negative ways. Shading and evapotranspiration facilitate cooling. Trees also lower wind speed and reduce advection, however, which may decrease the cooling effect. In addition, during nighttime, tree canopies inhibit long-wave radiative cooling by blocking part of the skyview, while excess moisture increases the thermal capacity of the soil and slows down surface cooling (Erell et al., 2012).

[4] The observed cooling benefit results are shown in chapter 2, page 20 and Figure 6.

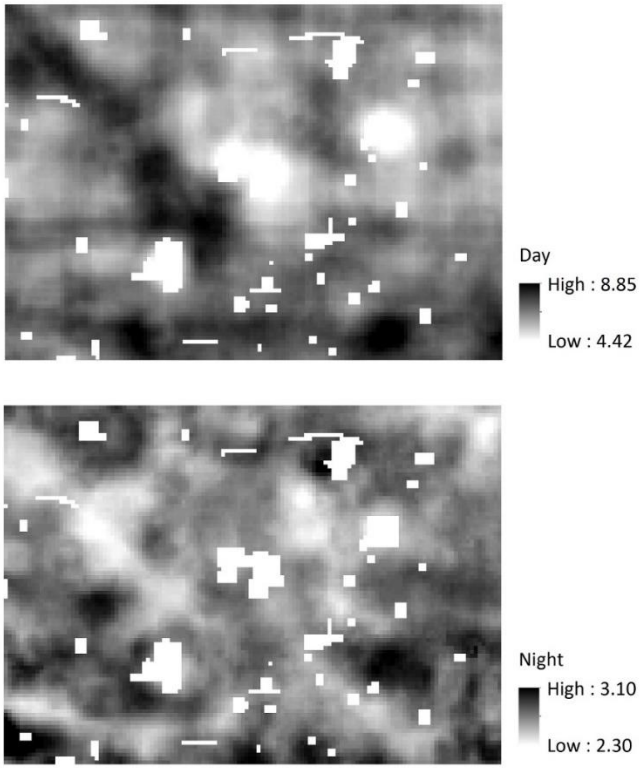

Figure 10. *Predicted Direct Cooling Benefits*

When area *i* is converted to green space, it also distributes indirect cooling benefits to neighboring land, eight areas in this case. The predicted indirect cooling benefit estimations are summarized in Figure 11 for the case of a single neighboring green space (k = 1, so δ_{i1}). The mean daytime and nighttime δ_{i1} are 2.7 °C and 1 °C, respectively. Spatially, Figure 11 is much patchier compared to Figure 10. The patchy pattern (steep values changes within a short distance) highlights potential cooling centers in the study area. For example, during the daytime, the local cooling centers are places that have a high percent of vegetation cover or complex shaped buildings within their neighborhood, and low percent of vegetation cover beyond. At nighttime, however, local cooling centers change to places that have high contrast between the percent cover and

shape of the paved surface within and beyond their neighborhood. While not shown here, multiple neighboring green spaces will enhance local cooling. This is reflected in the cases when $k \geq 2$ for δ_{ik}.

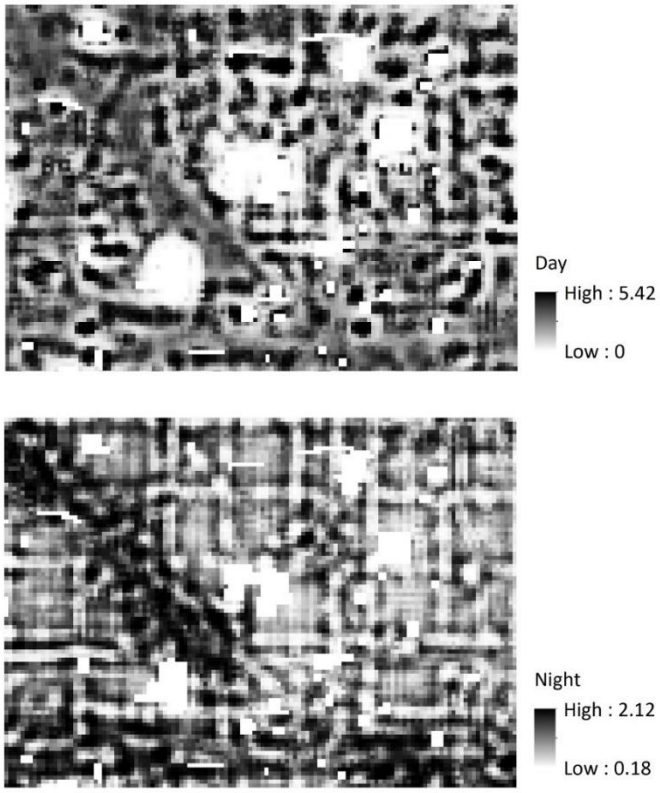

Figure 11. *Predicted Indirect Cooling Benefits (*k*=1 case)*

3.4.2 Day-Night Cooling Trade-offs.

The optimization model allows for any level of green space allocation to be evaluated, but the results presented here are necessarily focused on the city's plan objective. Consequently, in this analysis it is assumed that 150 land units will undergo conversion to green space, thus p = 150. This equates to 121.5 ha of new green space (1.3% of the study area). Table 9 summarizes the trade-off solutions identified when the

importance weight for day and night cooling benefits is varied. When w = 1, daytime cooling benefits are considered to be the most important. The result, Ω_{day}, corresponds to 5,479.80 °C in total temperature reduction across all cells in the study area. Associated with this allocation of green space, the nighttime cooling benefit is 1,908.02 °C in Table 9. Alternatively, when w=0, this represents the case where nighttime cooling benefits are deemed most important, and the objective value, Ω_{night}, is 2,233.94 °C. Associated with this pattern of green space would be a total daytime cooling benefit of 4,738.28 °C. These two situations highlight that optimizing daytime benefit is not equivalent to optimizing nighttime benefit. As such, compromise green space selection solutions can be identified that consider both day and night cooling benefits simultaneously by varying the value of w, reported in Table 9.

Table 9

Day-Night Trade-off Solutions

w	Ω_{day}	Day: % of obj. decreased	Ω_{night}	Night: % of obj. decreased
1	5479.80	0.00%	1908.02	14.59%
0.9	5479.27	0.01%	1917.52	14.16%
0.8	5476.91	0.05%	1931.42	13.54%
0.7	5466.80	0.24%	1959.69	12.28%
0.6	5442.68	0.68%	2002.95	10.34%
0.5	5401.44	1.43%	2053.49	8.08%
0.4	5328.01	2.77%	2110.58	5.52%
0.3	5256.25	4.08%	2148.13	3.84%
0.2	5111.26	6.73%	2194.82	1.75%
0.1	4957.13	9.54%	2221.46	0.56%
0	4738.28	13.53%	2233.94	0.00%

Figure 12 depicts the trade-off solutions of the Ω_{day} and Ω_{night} columns in Table 9 for each value of w. Included in this figure are distributions of three trade-off solutions,

where the w = 1 (importance on daytime cooling benefits) green space pattern is shown closest to the x-axis, the w = 0 (importance on nighttime cooling benefits) green space pattern is shown closest to the y-axis, and the w = 0.3 pattern is in between. The latter is a compromise between the two competing objectives. The patterns vary spatially, which is not surprising considering the variation reflected in simulated cooling benefits detailed in Figure 11.

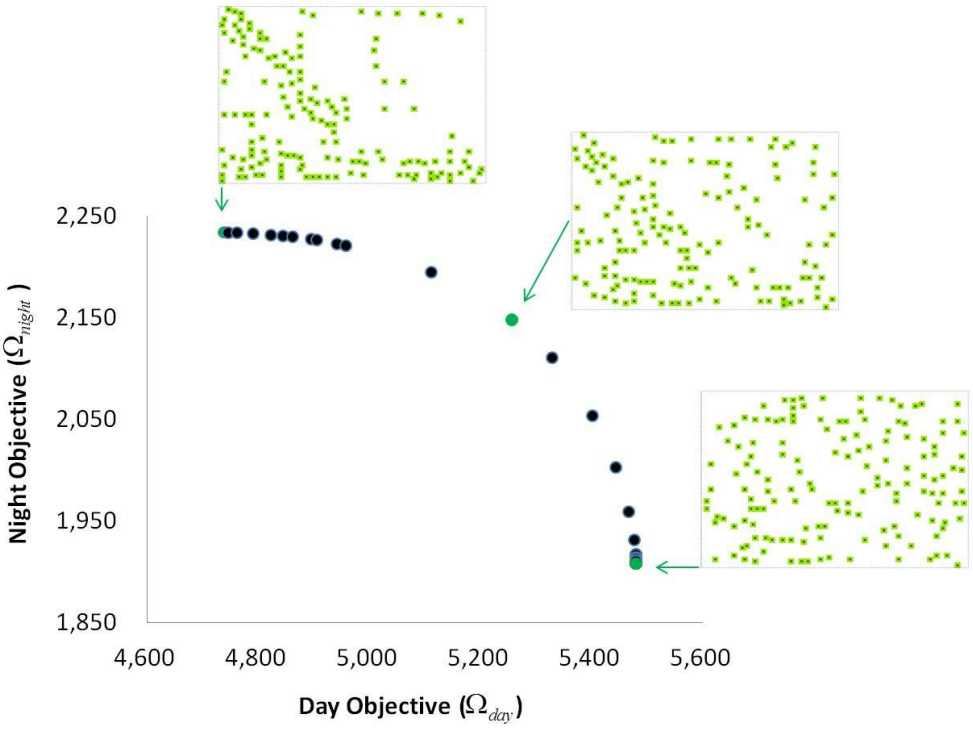

Figure 12. *Day-Night Trade-off Solutions*

The optimal green space allocations lead to dramatic gains in local cooling benefits. Day conditions resulted in direct and indirect benefits of 6.68 °C and 3.74 °C on average, respectively, which is about 2 °C higher than means for observed, existing green space cooling benefits in the study area. Similarly, night condition local cooling benefits were able to increase some 1 °C to 2.57 °C and 1.55 °C (direct and indirect, respectively) on average. Beyond this, a significant drop in regional average temperature across the

study area is also observed. The mean observed temperature in the study area is 55.60 ℃ and 29.85 ℃ for day and night, respectively (Fig. 7). The greatest reduction in average temperature during the day is associated with the green space pattern when w = 1, reducing temperature to 55.13 ℃. This represents almost 0.5 ℃ less than the current average in the study area of 55.60 ℃. The greatest reduction in nighttime average temperature is the green space pattern when w = 0, reducing temperature to 29.66 ℃ (a 0.19 ℃ decrease from current average temperature). This is remarkable given that the new green space was limited to only 1.3% of the study area. There may well be increased benefits if more green space is considered. Other research beyond Phoenix indicates that a similar reduction in air temperature, to which LST contributes, leads to a decrease of up to 10% in peak energy demand (Fung et al., 2006; Meier & Taha, 2000). Trade-off solutions, therefore, range between these extremes. For the green space pattern when w = 0.3, the average daytime temperature is 55.15 ℃ and the nighttime average temperature is 29.67 ℃.

The spatial heterogeneity of cooling benefits associated with green space allocation solution is depicted in Figure 13 for the case when $w = 0$ (importance on nighttime cooling). This illustrates not only where the green space is to be located, but also the derived direct and indirect cooling benefits. The selected locations are consistent with existing findings on nighttime SUHI, which suggest that areas of abundant impervious cover have a higher impact on cooling than vegetated area at night (Buyantuyev & Wu, 2010; Myint et al., 2013). As demonstrated in Figure 13, places along the industrial corridor and nearby the airport have the highest potential for nighttime cooling. In contrast, highly vegetated neighborhoods observe minimal new

green space allocation. Of note is the agglomeration of indirect cooling benefit captured in this case (inset image shown in Fig. 13). The overlapped neighborhood received 0.6 °C higher cooling than the single coverage neighborhood. It proves beneficial to ensure in this case that indirect local benefit is enhanced. That is, capturing the contribution of local benefits ($k \geq 2$) is favored. The model is able to strategically account for this in order to maximize regional cooling benefits.

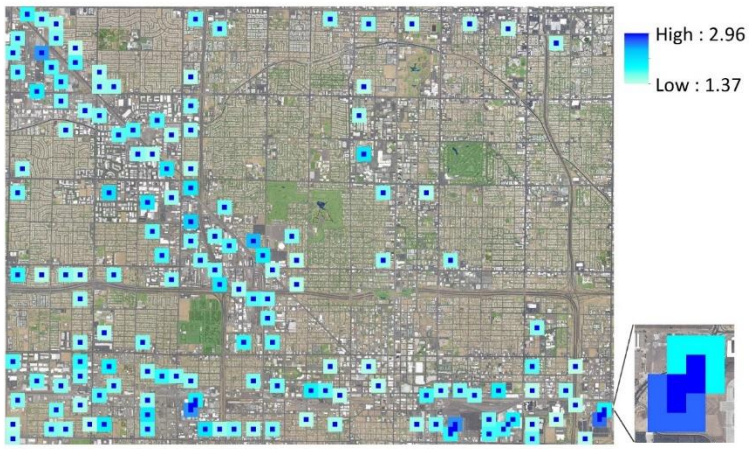

Figure 13. *Green Space Allocation Pattern (w=0)*

3.5 Discussion

It is well known that increasing green spaces in urban areas helps to ameliorate the extremes of UHI and SUHI effects. The research dedicated to this relationship has largely focused on the amount or area of green spaces, although increasing attention has focused on the broader characteristics of the pattern of green spaces such as concentration or dispersion (Myint et al., 2015). To our knowledge, however, no attempts have been made to determine the optimal locations for green spaces accounting for local UHI variations, creating an information lacuna for decision makers confronting the negative

impacts of excessive urban temperatures (e.g., Hondula et al., 2014). Our framework effectively addresses this issue by integrating GIS, remote sensing and spatial statistics with optimization modeling. The model links green space allocation with local landscape context and enables identification of trade-off solutions that balance diurnal cooling benefits.

3.5.1 General Implications of UHI Reduction.

The results suggest that optimal green space siting may lead to 1 to 2 °C local LST reduction and nearly 0.5 °C regional LST reduction, on average, throughout the Phoenix study area. This is remarkable given that the new green space was limited to only 1.3% of the study area. There may well be increased benefits if more green space is considered. Other research beyond Phoenix indicates that a similar reduction in air temperature, to which LST contributes, leads to a decrease of up to 10% in peak energy demand (Fung et al., 2006; Meier & Taha, 2000). The consequences for water use are more complex, however. Green spaces, such as the turf grass assumed in this study, require substantial water in desert cities. All turf grass and non-native vegetation in Phoenix is irrigated, and outdoor water application currently accounts for a majority of residential and neighborhood water use in the metropolitan area (Balling & Gober, 2008; Gober et al., 2009; Wentz et al., 2016). As a result, adding more green space may increase water demand, but the rate of use might be lowered by incorporating mixed vegetation. Research in the Negev Desert in Israel, for example, found that a combination of grass covered by shade trees or mesh shading created a synergy with greater cooling and led to a 50% reduction in water use (Shashua-Bar et al., 2009). Finally, ameliorating

temperature extremes is known to have positive health impacts (e.g., Hondula et al., 2012).

3.5.2 Trade-offs of Green Space Cooling.

Beyond temperature reduction, this study also provides valuable insights on green space patterning in relation to cooling trade-offs. Our finding is consistent with existing research that the concentration of green spaces enhances local cooling (Chang et al., 2007; Spronken-Smith & Oke, 1999). Such observations, however, do not consider the trade-offs between local and regional cooling benefits. Our model demonstrated that, although clustered pattern enhances local cooling, their overall regional cooling benefit is lower than the spatially dispersed pattern (Fig. 13). This is because the dispersed pattern ultimately influences a larger area through the local cooling provided to adjacent parcels of land. In addition, other studies in the Phoenix area have observed the varied diurnal role of different land-covers on SUHI (Buyantuyev & Wu, 2010; Myint et al., 2013). As of yet, however, minimal attention has been given to the evaluation of trade-offs between day and night relative to an established pattern of land-cover. Our modeling approach addresses this, indicating that maximized daytime cooling of green spaces results in an approximately 15% reduction in nighttime cooling and vice versa. Optimizing for both day and night simultaneously, it is possible to achieve some 96% of the potential cooling benefits.

3.5.3 Limitations and Future Research Avenues.

The model results are significant and point to the utility of such approaches. Our framework, however, is a first-generation effort and as such has a number of limitations that require attention in future research. For example, distance decay patterns of the

cooling benefit were simplified to an "all or nothing" coverage assumption based on a fixed cooling extent. Future development could relax this assumption using a general coverage function representing the proportion of cooling benefit obtained at a certain distance from the green space (see Berman et al., 2010). In addition, an isotropic surface temperature distribution was employed, in which the temperature is represented by its mean value within a given area. In reality, the cooling effect varies spatially in different directions, which would potentially affect the extent and the interactions of cooling among adjacent green areas (see Lin et al., 2015). It is also worth noting that indirect cooling benefits could be more extensive than represented in the modeling framework. It is likely that our approach has underestimated the indirect cooling benefits, δ_{ik}, which may have implications on the spatial pattern of optimal green spaces. Further study requires more adjacent green space samples to better quantify indirect cooling. In this case, linear modeling is employed to better interpret variable effects. In general, then, it is clear that estimation of direct and indirect benefits is an important area for future research, both in terms of the quality of estimates but also in terms of green space selection impact. For example, the non-linear relationship between cooling benefit and the size of green space has been reported in several studies (Cao et al., 2010; Chang et al., 2007).

On the modeling side, parameter value changes and sensitivities could also be explored. As noted previously, more new green space could be considered, which would involve increasing the parameter p and re-running the optimization models. The relationship between green space allocation and regional temperature response certainly is an area for more research.

3.6 Conclusions

Our integrated framework demonstrates significant cooling potentials can be gained through optimal green space placement in Phoenix, Arizona. Both daytime and nighttime cooling effects are examined because of their combined impacts on human well-being, energy and water use, and environmental performance. The selected optimal locations enhance landscape heterogeneity at the local-scale, which would increase the surface temperature gradients and potentially accelerate air flow, preventing daytime heat storage and facilitating nighttime cooling. In addition, 96% of the potential day and night cooling benefits can be achieved through simultaneous consideration. The results also demonstrate that clustered green space enhances local cooling because of the agglomeration effect; whereas, dispersed patterns lead to greater overall regional cooling. The developed model can be further applied to assess different land arrangements for various cooling considerations. Our findings help to address the growing environmental problem of extreme temperatures confronting urban areas worldwide.

CHAPTER 4

EVALUATING THE EFFECTS OF VERTICAL URBAN FORMS ON LAND SURFACE TEMPERATURE USING GOOGLE STREET VIEW

4.1 Introduction

Numerous flat or planar surface assessments demonstrate the consequences of the composition and configuration of urban land-cover (i.e., land system architecture [Turner, 2017]) on land surface temperature (LST) and above-ground air temperature for Phoenix, Arizona (Li et al., 2016; Myint et al., 2013; Kamarianakis et al., 2017). For the most part, these works demonstrate that the compactness of individual land-cover patch and the clustering of the same patch type can increase or decrease diurnal temperatures, depending on the land-cover type. The built urban environment, however, is repeat with vertical structures (i.e., buildings, trees) that affect climate within the canopy layer in various ways, such as shading, wind tunnels, and sky view. This vertical dimension is central to research on turbulence and flux dynamics as undertaken in urban climatology (Unger, 2004, 2009; Coseo & Larsen, 2014).

Planar surface assessments account for a full array of land-covers (e.g., building, tree, and impervious and soil cover). Significantly, though, common vertical indicators often do not discriminate among different land-covers. Buildings and tree canopies affect temperature through different mechanisms, for example, but are not necessarily made distinct in vertical dimension assessments (Unger, 2009). Interestingly, Google Street View possesses an immense collection of street panoramas, providing information on surface properties that include the differences in the vertical dimension objects, the

heterogeneity of which is large in an urban context (Carrasco-Hernandez, 2015, Middel et al., 2017; Li et al., 2018).

The research presented here examines diurnal variation in LST for the city of Phoenix, Arizona, by combining the 1 m planar land-cover map with the vertical urban forms. It does so by employing spherical fractions of different surface classes created from Google Street View images. In addition, to capture other potential contributors to LST variations, additional factors like yard preferences and maintenance (Chow & Brazel, 2012; Larson et al., 2009) and social variables, such as income and parcel construction year, are employed in the analysis. Finally, while most LST studies have assumed spatially stationary relationships and have relied on global model estimates, Su and colleagues (2012) examined the relationships between urban land-cover and LST using the geographical weight regression and concluded that a conventional global model underestimates the surface-UHI (SUHI) at the local-scale. Based on the above, this research addresses three questions:

1. What are the differences between the spherical and planar land-covers at the local-scale?
2. To what extent do the spherical fractions contribute to the LST variations in day and night?
3. How do the relationships between LST, urban form, and social variables vary locally during day and night?

4.2 Data

4.2.1 Land Surface Temperature.

Land surface temperature was derived from Advanced Spaceborne Thermal Emission and Reflection Radiometer (ASTER) data layers. The ASTER image consists of six bands for short-wave infrared, at 30 m resolution, and five bands of thermal infrared, at 90 m resolution (Yamaguchi et al., 1998). Its multiple thermal wavelength channels facilitate surface emissivity estimation using multispectral methods. The surface temperature measurements were derived from the ASTER_08 product. These data contain surface readings in Kelvin, corrected for atmospheric transmission, emissivity, absorption, and path radiance (Gillespie et al., 1998). The absolute accuracy of the measures ranges from 1 to 4 K, with a relative accuracy of 0.3 K (JPL, 2001). In order to address the summer diurnal temperature variation, a pair of night and day cloud-free images were selected for July 29, 2014 (22:00 at local time) and May 31, 2015(11:00 at local time) considering data availability constraints (Fig. 14). Based on the information from the Phoenix Sky Harbor weather station, both dates had clear and calm weather with no precipitation and were representative of the typical summer conditions. The daily mean air temperature on July 29, 2014 was 38.13°C and the mean humidity, 23.4%. The daily mean temperature on May 31, 2015 was 34.35°C, and the mean humidity, 13.5%.

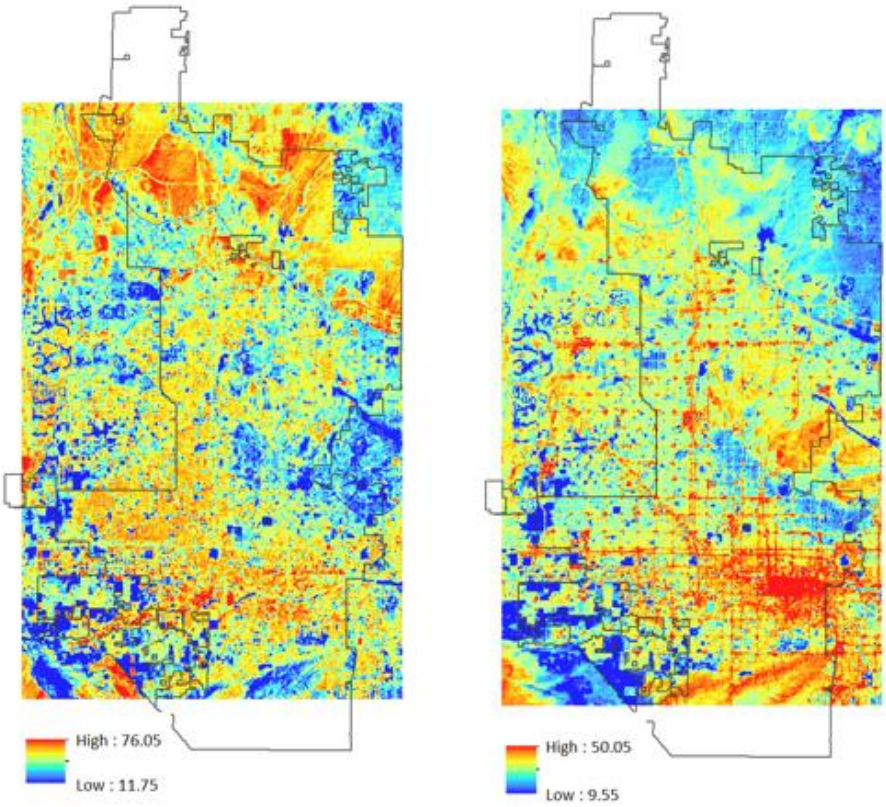

Figure 14. *Day and Night Land Surface Temperature (in °C)*

4.2.2 Planar Land-Cover Map.

A 1 m land-cover map was created using aerial imagery from the National Agricultural Imagery Program (Fig. 15.a). The data have four bands (RGB and NIR) and were acquired for summer 2010. The images were classified using the object-based method, implemented using the eConigtion software (Li et al., 2014). The resulting land-cover data layer included 12 land-cover classes with an overall accuracy of 91.9%. For the purposes of this analysis, the 12 land-cover classes were aggregated into six: building, paved surface, soil, tree (including shrub), grass, and water. The resulting 1 m land-cover data avoids the mixed feature problem of low-resolution data. Thus, it effectively depicts

small, fragmented patches and enables examination of individual land-cover effect on LST variations.

4.2.3 Spherical Fraction from Google Street View.

The spherical land-cover fraction was created following three steps: Google Street View image acquisition, image segmentation, and spherical fraction computation. The images were requested through Google Street View image API (application programming interface) based geographical coordinates along the streets. For each coordinate point, street images in six directions were acquired (N-S-E-W, up, down) and composed to a photo cube. In the segmentation step, an instance of the fully convolutional network (FCN) developed by Long and associates (2015) was trained to segment the photos into six classes: sky, trees, buildings, impervious surfaces, pervious surfaces, and moving objects. To improve classification accuracy, the network was trained for three different view directions: lateral, down, and up. The classified image cube was projected onto a unit sphere, mimicking how a person experiences the urban environment in a street canyon. Finally, the areal fraction of each class on the unit sphere was computed based on the spherical excess. The overall accuracy of the spherical dataset is 95%, enabling fine-scale evaluation of the vertical urban form (Lukasczyk et al., nd).

The total number of 1.6 million photo cubes were retrieved for the study area. Figure 15.b - d show spatial patterns of spherical fractions for building, sky, and tree. The spherical data points are distributed densely along the street network, with an average distance of 2 m. Building fraction for most of the city is relatively low, ranging from 5% to 18%. Only the city center has higher building fractions above 20%. Tree fraction varies greatly across the study area, ranging from 5% to 36%. Sky fraction is generally

high in this area (above 30%), and shows inverse spatial pattern compared to that of tree and building.

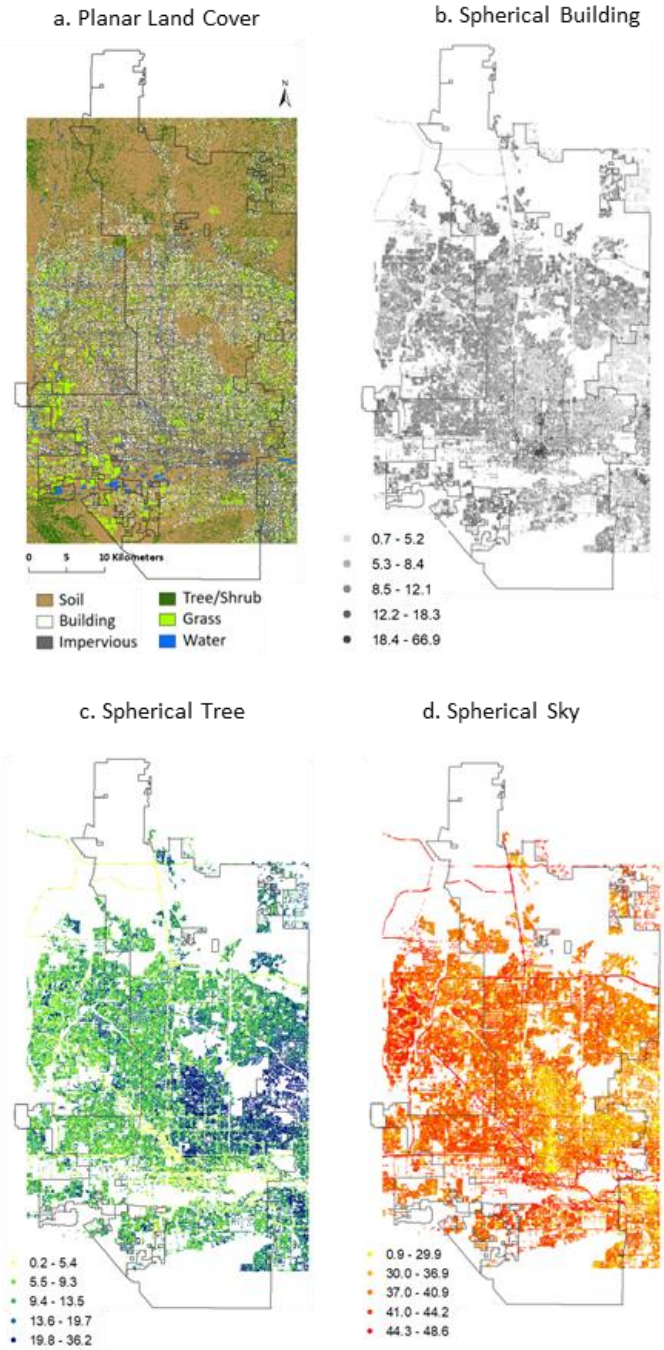

Figure 15. *Planar and Spherical Maps*

4.2.4 Social Variables.

The social demographical data at the census tract level were acquired from the 2015 American Community Survey 5-year estimates. It provides updated annual data compared to the 2010 Decennial Census. Variables noted in other work to affect LST were employed (Larson et al., 2009; Harlan et al., 2006; Li et al., 2016). They include population density, number of households, % of Hispanic, median household income, median resident's age, and parcel construction year. The mean construction year of each census tract was calculated based on 2016 parcel level cadastral data from the Maricopa Association of Governments. The fine-scale land-use data of the area in 2010 and 2015 were also acquired from the same source.

4.3 Methods

4.3.1 Comparison between the Spherical and Planar Fractions.

Compared to the planar dataset, the spherical dataset has different viewing angles. In addition, its field of view varies by street geometry, and the objects within adjacent street view images may overlap with each other. Several urban climate studies have suggested that compared to single site or pixel value, areal mean of the appropriate-sized area better represents local environment conditions (Stewart, Oke, & Scott 2013; Unger, 2009). Based on the local climate zones classification in Phoenix metropolis, the areal mean values at the census tract level were used in this study (Wang et al., 2018). Due to the year differences between the planar and the spherical datasets, specific areas or views that had changed from 2010 to 2015 were removed. In addition, Google Street View does not cover green and open lands, so these areas were also excluded in subsequent analysis to make the two datasets comparable.

Because the spherical fraction is point-based, both the mean and standard deviation statistics can be computed. For the planar fraction map, however, only mean statistics are available. Notation $U_{m,n}$ represents the different variables. *U* indicates the six land-cover classes, *m* represents the spherical or planar dataset, and *n* indicates mean or standard deviation. For example, $building_{P,M}$ denotes the mean value of planar building class, otherwise, $building_{S,SD}$ indicates the standard deviation of spherical building class. Paired t-test and box-plot are used show the differences between the two types of fractions.

4.3.2 Correlation and Global Regression Analysis with LST.

The Pearson's correlation analysis is utilized to assess the associations between the spherical and the planar fractions with daytime and nighttime LST. The multiple ordinary least square (OLS) regression is employed to create the global models of LST. In order to understand the individual and jointed contributions of the two types of fractions on LST variation, four groups of inputs variables are examined. Group 1 contains only the planar variables, group 2 contains only the spherical variables; group 3 combines variables from both datasets, and group 4 contains additional social variables in addition to that of group 3. Considering the large number of input variables, a forward stepwise method is used to avoid model overfitting and select the most parsimonious variable set of each group.

4.3.3 Local Regression Analysis with LST.

A wide range of regression techniques were developed to modeling spatial data (Anselin, 2002; Charlton, Fotheringham, & Brunsdon, 2009). For example, the spatial lag and spatial error models are typical methods to address spatial dependence, the

phenomenon that nearby locations will have similar values (Tobler, 1970). They deal with the spatial structure present in the residual or in the variables and find the unbiased parameter estimates using the maximum likelihood estimation (Anselin, 1988). On the other hand, geographically weighted regression (GWR) is designed to examine spatial heterogeneity, the phenomenon that the relationship between variables is not stationary, but changes over space (i.e., the changes of spatial dependence over space). Extended based on the ordinary least squares (OLS) regression, GWR preserves the coefficient interpretability. It is useful as an exploratory technique to visualize how the relationship between the spherical and planar fractions and the LST varies in space. Specifically, GWR allows the parameter estimates to vary spatially based on an optimally selected bandwidth, assuming that there are *m* number of predictors ($j \in \{1,2,\ldots,\mathrm{m}\}$) and *n* number of observations. For observation $i \in \{1,2,\ldots,\mathrm{n}\}$ at location (u_i, v_i), the linear formation of the model is:

$$y_i = \sum_j \beta_j (u_i, v_i) x_{ij} + \varepsilon_i \quad (13)$$

Where y_i is the response variable, x_{ij} is the jth predictor variable, $\beta_j (u_i, v_i)$ is the jth coefficient, and ε_i is the error term (Fotheringham, Brunsdon & Charlton, 2002). The GWR4 software is used to implement the method. The corrected Akaike Information Crtierion (AICc) is used to compare the model fit of the global OLS model with the local GWR model that have identical predictors (Charlton, Fotheringham, & Brunsdon, 2009). To determine whether parameters are locally significant, the critical value α for t-test needs to be adjusted for the multiple hypothesis testing (da Sliva & Fotheringham, 2015).

4.4 Results and Discussion

4.4.1 Comparisons between the Spherical and Planar Fractions.

Table 10 shows the descriptive statistics of the spherical and planar factions at the census tract level. Among the planar fractions, soil and impervious have the largest mean values, approximately 30%, followed by building (21%), and tree and grass (15%). In terms of the spherical fractions, sky and impervious have the largest mean values, close to 40%. Together, they account for nearly 80% of the entire sphere. The mean values of tree and building are approximately 10%. Pervious surface, which mainly consists of grass, bare soil, or gravel, has the smallest mean value, only accounting for 3% of the sphere. The standard deviation of each spherical fraction indicates their heterogeneity within each census tract. Among the spherical fractions, tree has the largest standard deviation (6%), followed by sky, building, impervious (ca. 4.5%), and pervious (2.4%).

Table 10

Descriptive Statistics of the Planar and Spherical Fractions

	Mean	**Std. Deviation**	**Min**	**Max**
Planar Mean				
Soil	30.8	9.9	3.2	65.4
Building	21.4	4.5	7.0	34.7
Tree	8.8	5.0	1.2	25.8
Grass	6.7	3.6	0.1	22.3
Impervious	31.9	11.3	4.5	68.0
Spherical Mean				
Sky	38.9	2.7	22.4	45.1
Building	8.1	2.0	2.0	29.5
Tree	11.9	3.5	4.7	25.8
Pervious	2.8	1.3	0.4	8.9
Impervious	36.4	1.7	28.7	41.5
Spherical Std.				
Sky	4.7	1.3	2.5	11.8
Building	4.5	1.6	2.1	12.3

Tree	6.0	1.5	3.3	12.3
Pervious	2.4	1.0	0.8	6.8
Impervious	4.2	0.9	2.7	9.2

The box-plot graphically shows the range and variance of the two types of fractions (Fig. 16). Compared to the planar fraction, spherical fractions have narrower ranges and variances, primarily because they are street-based. Based on the above statistics, the paired t-test table further compares the mean differences between the building, tree, and impervious classes (Table 11). All three pairs show significant mean value differences between the two datasets, revealing the distinct differences between the horizontal and the vertical urban form. For example, planar building indicates the roof fraction; in contrast, spherical building represents the wall fraction. In the results, the roof fraction is significantly larger than the wall fraction by 13.3%, and the two show no associations. On the other hand, the tree and impervious classes of the two datasets are significantly correlated.

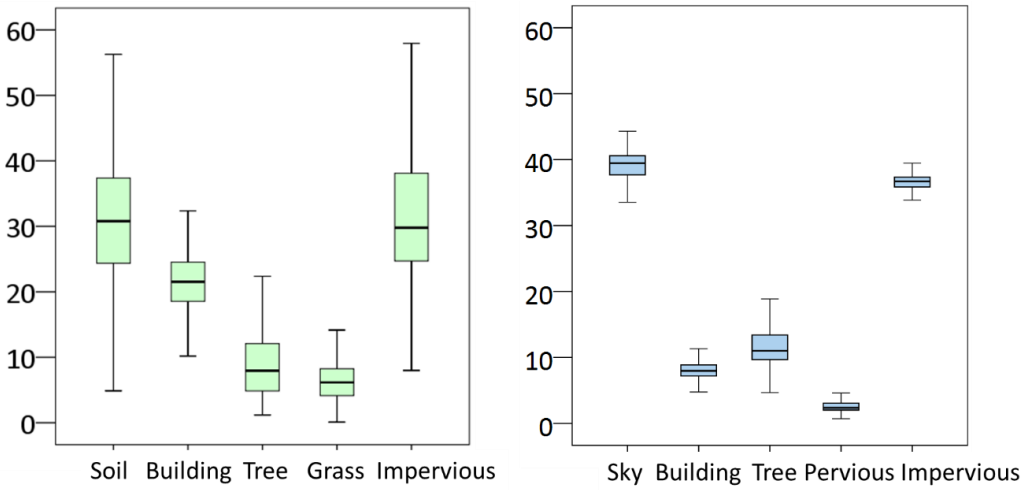

Figure 16. *Planar and Spherical Fractions Boxplots*

Table 11

Paired T-test of the Planar and Spherical Fraction Differences

	Planar	Spherical	Correlation Coeff.	Paired Differences	
				Mean	Std. Deviation
Building	21.4	8.1	.06	13.3**	4.8
Tree	8.8	11.9	.48**	-3.1**	4.5
Impervious	31.9	36.4	.33**	-4.4**	10.8

4.4.2 Correlation of the Spherical and Planar Fractions with LST.

Correlation of the two datasets with LST were tested (Table 12). Results of the planar fraction are in line with previous research findings. Tree and grass have strong negative effects on LST during the day and at night. Impervious surface has strong positive effects on LST, especially at night (Zhou et al., 2011; Li et al., 2016; Myint et al., 2015). Building (roof) positively associates with LST during the day and negatively affects LST at night because it heats and cools faster compared to the ground surface (Oke et al., 2017). In the desert environment, dry soil cools faster at night, thus soil is negatively correlated with nighttime LST (Imhoff et al., 2010).

In terms of the spherical fraction, the mean values of all the classes show significant correlation with LST, demonstrating the critical role of vertical urban form in daytime and nighttime LST variation. Specifically, tree and pervious surface have strong negative correlations with LST. Sky, building, and impervious surface show a positive association with LST. Interestingly, sky strongly affects daytime LST (0.53**) but weakly affects nighttime LST (0.11**). Compared to sky and impervious, building has a weaker effect on daytime LST (0.24**) but stronger effect on nighttime LST (0.35**).

This is in line with Liu and colleagues (2017) that building wall has positive correlation with LST at doth daytime and nighttime in different seasons. The majority of the spherical standard deviations are significantly correlated with LST, indicating heterogeneity of the vertical form also strongly affects LST. During the daytime, standard deviations of all the classes are negatively correlated with LST. This suggests that increases vertical form heterogeneity, especially for trees, can effectively reduce daytime LST, which has not yet been examined. Daytime correlations are ranked as tree > pervious > sky > impervious. At night, $building_{S,SD}$ has the strongest positive effect on nighttime LST (0.36**), suggesting that larger vertical heterogeneity of building increases LST at night.

Table 12

Pearson Correlation Analysis of the Planar and Spherical Fractions

Planar	Day LST	Night LST
Mean		
Soil	-.05	-.30**
Building	.10*	-.16**
Tree	-.51**	-.36**
Grass	-.37**	-.28**
Impervious	.36**	.58**
Spherical	Day LST	Night LST
Mean		
Sky	.53**	.11*
Building	.24**	.35**
Tree	-.64**	-.40**
Pervious	-.50**	-.51**
Impervious	.40**	.42**
Std. Deviation		
Sky	-.31**	.17**
Building	-.07	.36**
Tree	-.45**	-.06
Pervious	-.43**	-.36**
Impervious	-.26**	0.01

4.4.3 Global and Local Regressions.

Table 13 summarizes the R^2 and adjusted R^2 of the four groups of global models. The adjusted R^2 takes into account the number of independent variables in the model and reflects model parsimony. Individually, spherical fraction performs better than the planar fraction in both daytime and nighttime. Due to the high sky view factor in Phoenix, the vertical form and shading conditions may be more effective in blocking the daytime shortwave radiation than the nighttime longwave radiation (Middel et al., 2014; Middel, Lukasczyk, & Maciejewski, 2017).

Employed jointly, the two types of fraction complement each other, explaining 57% of the daytime LST variation and 51% of the nighttime variation. Finally, adding social

variables significantly improves the daytime model; the R^2 increases from 0.57 to 0.71. The R^2 of nighttime model slightly increases from 0.51 to 0.52. In summary, daytime models have better model fit (i.e., higher R^2) than nighttime models. This result is consistent with previous planar remote sensing assessments. Because of generally stronger land-cover—LST relationships during the day, peak temperatures may be more easily managed than nighttime minimum temperatures through landscape modification (Jenerette et al., 2015).

Table 13

R^2 and the Adjusted R^2 of Global Regressions

Global regression		**Planar**	**Spherical**	**Planar + Spherical**	**Planar + Spherical + Social**
Day LST	**R^2**	.38	.48	.57	.71
	Adj. R^2	.37	.47	.56	.70
Night LST	**R^2**	.37	.39	.51	.52
	Adj. R^2	.37	.39	.50	.52

The daytime model 4 was the most robust global model. Therefore, its input variables were imported into GWR4 software to create the local model and uncover the spatially varied relationships with LST. Table 14 lists the global and local model results. Compared to the global model, the R^2 of the local model increases from 0.71 to 0.85, and AICc value drops from 1188 to 1067, both indicating better model fit. As a relative measure, the difference between AICc values is important. Smaller AICc indicates a better model fit (Hurvich, 1998). Furthermore, residuals of the global model show a weak but significant spatial autocorrelation, with a Moran's I value of 0.2*. In contrast, residuals from the local model have no sign of spatial autocorrelation (Moran's I is 0.005). The bandwidth of the local model indicates the optimal number of neighboring

census tracts used in the local regression. Compared to the total number of census tracts, 474, a bandwidth of 85 demonstrates the scale of local variation.

Table 14

Local and Global Regression Parameters

	Local - GWR	**Global - OLS**
R^2	.85	.71
AICc	1067	1188
Residual's Moran's I	.005	.2*
Bandwidth	85	474

Figure 17 lays out the spatial varied patterns detected by the local model, including distributions of the local R^2, variables coefficients, and the number of significant variables per census tract. In general, the local R^2 ranges from 0.52 to 0.93 with a mean value of 0.85. The majority of the urban area has better model fit with a R^2 above 0.65; the northern suburban area has lower model fit (Fig. 17.a). Figure 17.c - f are local coefficient maps, the colored areas indicating where the parameter is significant at α = 0.05 level (the adjusted α' is 0.0034). The black-white map shows the distribution of the corresponding variables. Local coefficients patterns highlight that the effect of urban form on LST is not uniform, but rather varies spatially. For example, in Figure 17.c, according to global model estimates, a 1% increase of the $Tree + Grass_{P,M}$ per census tract reduces LST by -0.05 °C throughout the study area. The local model, however, reveals that for some highly vegetated census tracts, a 1% increase of the $Tree + Grass_{P,M}$ reduces LST by -0.13 °C. This result is in line with the suggestion that uniform landscaping plan is unsuitable to address the increasing LST across the entire city, and local variations should be discriminated carefully for efficient heat mitigation (Gober et al., 2010). In addition, Figure 17.d of the global model suggests a 1% increase of the

$Sky_{S,M}$ will lead to 0.12 °C increase in daytime LST across the study area. In fact, the local model illustrates for certain census tracts, a 1% increase of the $Sky_{S,M}$ will lead to 0.4 to 0.6 °C increase in daytime LST. Consequently, for those areas, increasing shade should be prioritized to minimize daytime LST.

Figure 17.b counts the number of significant variables per census tract. This map classifies Phoenix into different areas based on their dominant LST predictors. For example, in area A, LST is affected by three variables, $Tree + Grass_{P,M,}$ $Tree_{S,SD,}$ and the parcel construction year. In contrast, in area B, LST is only affect by $Tree_{S,SD,}$ and the parcel construction year. This indicates that increasing vegetation cover can significantly reduce LST in region A but not in region B. In region B, however, increased tree canopy diversity, which changes the shading condition, reduces LST. The local model results point to locations where specific landscaping style has the largest cooling potential. In summary, compared to the conventional global model, the spatially varied patterns from the local model make it easier to uncover the underlying thermodynamic process (Fotheringham, Brunsdon, & Charlton, 2002). Finally, the census tracts with zero number of significant variable indicate none of six variables is effective in explaining LST change. In this case, other factors should be tested to fully understand the LST variations in these places.

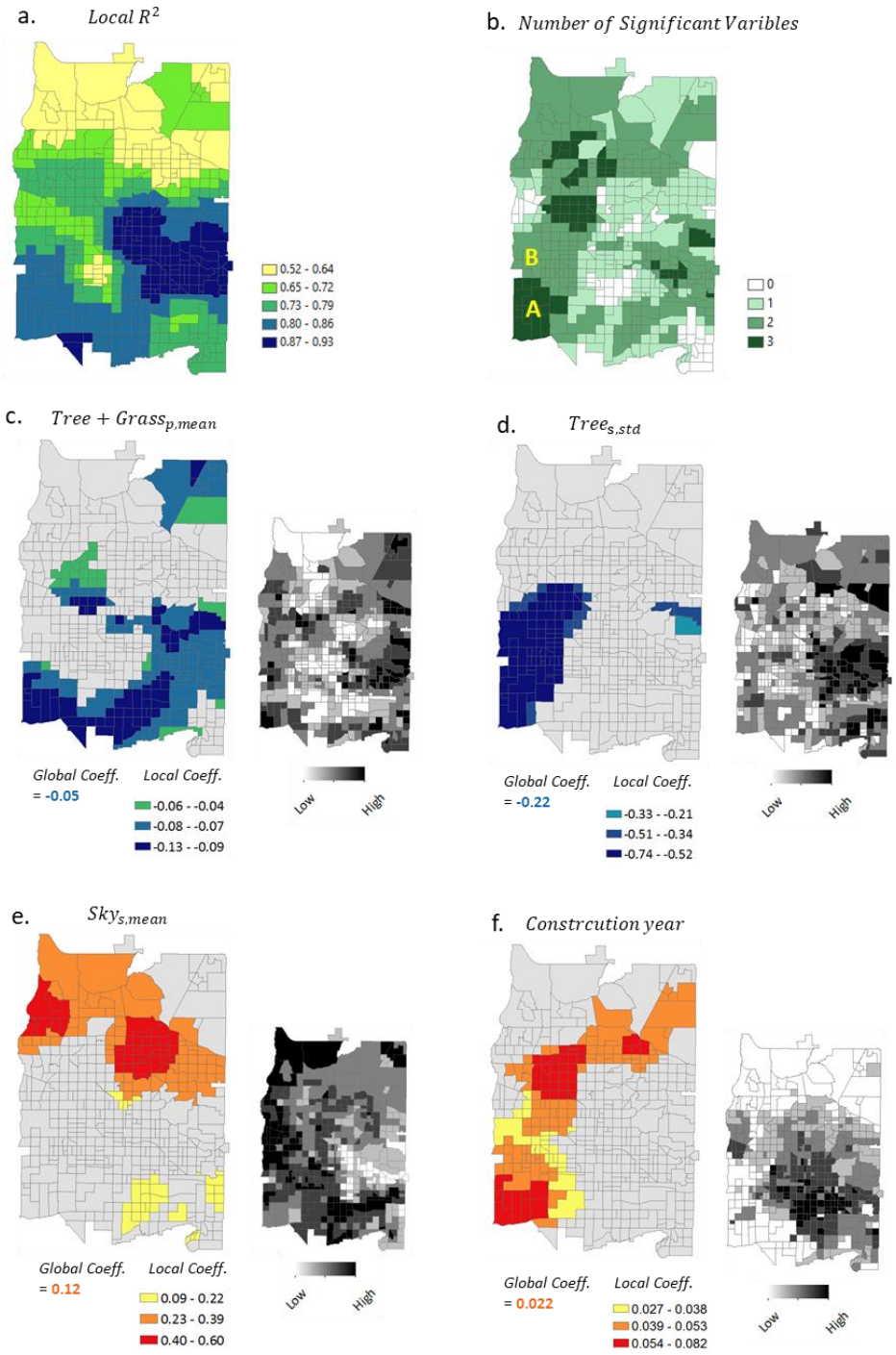

Figure 17. Geographical Weighted Regression Spatial Patterns

4.5 Limitations

Although GWR has been widely used for spatial pattern diagnostics, it suffers from the problem of multicollinearity. Wheeler and Tiefelsdorf (2005) used simulated data to demonstrate that GWR coefficients were potentially collinear even if the underlying variables in the data generating process are uncorrelated. This may introduce false positive spatial pattern when the true underlying process is stationary, which will affect local pattern validity. Therefore, spatial patterns resulting from GWR should be interpreted with caution. Future studies may use ridge regression or the least absolute shrinkage and selection operator (LASSO) regression to reduce the correlation among the coefficient estimates (Czarnota, Wheeler, & Gennings, 2015).

4.6 Conclusions

LST directly responds to diurnal surface (incoming and out-going) radiation exchanges which are strongly influenced by shading conditions and vertical urban forms. The metropolitan-wide assessment of Phoenix area demonstrates this urban climatology axiom. By adding vertical urban form to the Phoenix assessment, LST is predicted more accurately, increasing the R^2 by 0.2 compared to the conventional planar faction approach. The novel spherical fractions derived from Google Street View allow the effects of different vertical surfaces to be examined separately. Specifically, sky fraction and tree canopy have a stronger impact on daytime LST, in contrast to building, which has a stronger effect on nighttime LST. The relationship between urban form, social variables, and LST were comprehensively examined using both global and local models. The geographically weighted local model significantly improved model fit (R^2 increased from 0.71 to 0.85) and addressed the issue of spatial autocorrelation. Finally, the local model

maps feature the areas where certain urban form changes are especially effective for heat mitigation, supporting the optimal design of urban form and water resource allocation to minimize hot summer temperatures.

CHAPTER 5

SUMMARY

5.1 Significance of Research

A long-held axiom of the geographical sciences holds that the spatial arrangements of phenomena affect their performance and outcomes. This dissertation extends this axiom to urban land-cover/form and land surface temperature through an examination of the surface urban heat island (SUHI) effect and urban cooling that integrates UHI research across land system science, landscape ecology, geodesign, and urban climatology. It develops (1) a method to connect the cooling effect of green spaces with the land-cover within and beyond their boundaries based on land surface temperature measurements, and (2) an optimization model of green space allocation to reduce daytime and nighttime temperatures in which 96% of the diurnal reduction can be achieved. In addition, (3) the dissertation demonstrates that conventional horizontal assessments of urban land-cover on land surface temperature can be significantly improved by adding the vertical dimension of the "urbanscape" using Google Street View and geographically weighted regression. The optimization effort is the first of its kind used to address cooling spaces, and the Google Street View approach constitutes a nascent research venture.

Beyond Phoenix, the UHI effect confronts metropolises worldwide but is especially a concern during summer in temperate and tropical climates where 75% of world population is concentrated, largely in urban configurations (Kottek et al., 2006; Oke et al., 2017, p.337). Land-use decisions are essentially energy and water use decisions. Residential area dominates urban land-use and tends to be more similar and

homogenous in cities across broad geographical regions compared to the landscape of the original natural ecosystem (Wheeler et al., 2017; Polsky et al., 2014). These similarities, adjusting for climatic differences, indicate that the data and methods employed in this dissertation should be useful for other metropolises worldwide, and that the findings in Phoenix are applicable to other cities in the American Southwest.

This research offers new analytical approaches and potentially provides information about the role of land system architecture with regard to questions of urban climatic conditions and sustainability. Urban form, of course, amplifies or attenuates general climate conditions, and in the process affects a large range of environmental services and human well-being (Turner et al., 2013; Turner, 2017; Grimm et al., 2008; Seto et al., 2017). The research presented in this dissertation provides methods that may be used to address the problems of urban heat and provides insights for planners and managers to employ from the micro- to local-scale regarding urban form for cities. Indeed, portions of this work have been presented to the managers of Phoenix and Maricopa County as a means to address sustainability questions noted by the Office of Scientific and Technical Information, U.S. Department of Energy (https://www.osti.gov/biblio/1073575).

5.2 Limitations and Future Work

Land surface temperature derived from remote sensing is the primary data source of all three research projects in this dissertation. Passive remote sensing of upwelling thermal radiance is an efficient way of measuring surface temperature. Urban areas, however, exhibit strong thermal anisotropy relative to natural landscapes. Therefore, the measurement of the urban surface temperature from remote sensing is biased due to its

limited field of view, viewing geometry and position (Roth, Oke, & Emery, 1989; Voogt & Oke, 2003; Krayenhofff & Voogt, 2016).

In addition, remote sensing based data often only provide discrete snapshots of land surface temperature, providing incomplete data on diurnal and seasonal changes. Song and associates (2017) use in-situ metrological measurements to assess the relationship between land surface temperature and near-surface air temperature in Phoenix, Arizona. The result demonstrates the hysteresis effect between the two, supporting measuring and modeling of temporal surface and air temperature changes at the micro-scale. As noted in Chapter 2, additional work is required to determine the underlying rationale for the LST-distance relationship found in this study and others. Besides temperature, other meteorological parameters should also be quantified in future when linking heat mitigation strategies to human health, for example, shading, humidity, airflow pattern, and ventilation are important for outdoor thermal comfort and street level landscape planning (Middel, Lukasczyk, & Maciejewski, 2017; Zhao, Sailor, & Wentz, 2018).

The combination of GIS and location optimization is at the forefront of advances in spatial analysis and addressing urban sustainability challenges (Murray, 2010; Turner et al., 2013). Chapter 3 provided an "ideal" scenario, assuming that the spaces identified for cooling could be made green. It did not consider land availability for green space conversion. Smith, Li, and Turner (2017) developed a systematic approach to identify different types of vacant land for potential greening and UHI mitigation in Phoenix, Arizona. Future simulations should incorporate vacant land availability to create a more accurate estimation of cooling potentials. Furthermore, this study only evaluates the

trade-off between the daytime and nighttime cooling, future models should consider trade-offs with water and energy use.

The last research project demonstrated the importance of vertical urban form in explaining land surface temperature variation using fine-scale Google Street View data. Similar to the sky view factor employed in urban climatology, the spherical fraction derived from Google Street View does not contain vertical height information. Specific building and tree heights information that can be obtained from Lidar data are needed to further test associations between various urban form measurements.

5.3 From Science to Decision-Making Tools

The land system architecture framework and local climate zone scheme are emerging areas of interdisciplinary research among the subfields addressed here. Various research continues to demonstrate the promise of this integration, such as the recent work by Kamarianakis and associates, (2017) revealing a strong correlation between air temperature and land system architecture indicators for residential neighborhoods. This empirical-based science increasingly provides insights into urban planning. For example, Wang and colleagues (2018) classified local climate zones for Phoenix and Las Vegas at 100 m resolution using Google Earth, Saga GIS and Landsat 8. They compared the surface temperature, sky view factor, and land-cover composition of the classified local climate zones, generating a range urban form adjustments for desert cities. Results of this kind, in turn, provide insights for the development of geo-design tools to support decisions making. Taken together, the impact of the research fields integrated into this dissertation remain in a youthful stage of development. We should expect major impacts in the near future as this kind of research advances.

REFERENCES

Anselin, L. (1995). Local indicators of spatial association — LISA. *Geographical Analysis*, *27*(2), 93–115.

Anselin L. (1988). Spatial econometrics: methods and models, *Dordrecht: Kluwer Academic Publishers*

Anselin, L. (2002). Under the hood: Issues in the specification and interpretation of spatial regression models. *Agricultural economics*, *27*(3), 247-267.

Arnfield, A. J. (2003). Two decades of urban climate research: a review of turbulence, exchanges of energy and water, and the urban heat island. *International Journal of Climatology*, *23*(1), 1-26.

Balling, R., Gober, P., & Jones, N. (2008). Sensitivity of residential water consumption to variations in climate: an intraurban analysis of Phoenix, *Arizona. Water Resources Research*, *44*(10).

Balling, R., & Lolk, N. (1991). A Developing Cool Island in the Desert? The Case of Palm Springs, California. *Journal of the Arizona-Nevada Academy of Science*, *23*(2), 93-96.

Bechtel, B., Alexander, P.J., Böhner, J., Ching, J., Conrad, O., Feddema, J., Mills, G., See, L. and Stewart, I., 2015. Mapping local climate zones for a worldwide database of the form and function of cities. *ISPRS International Journal of Geo-Information*, *4*(1), pp.199-219.

Berman, O., Drezner, Z., & Krass, D. (2010). Generalized coverage: New developments in covering location models. *Computers & Operations Research*, *37*(10), 1675-1687.

Bowler, D. E., Buyung-Ali, L., Knight, T. M., & Pullin, A. S. (2010). Urban greening to cool towns and cities: A systematic review of the empirical evidence. *Landscape and Urban Planning*, *97*(3), 147-155.

Brazel, A., Selover, N., Vose, R., & Heisler, G. (2000). The tale of two climates Baltimore and Phoenix urban LTER sites. *Climate Research*, *15*(2), 123-135.

Buyantuyev, A., & Wu, J. (2010). Urban heat islands and landscape heterogeneity: linking spatiotemporal variations in surface temperatures to land-cover and socioeconomic patterns. *Landscape Ecology*, *25*(1), 17-33.

Ca, V. T., Asaeda, T., & Abu, E. M. (1998). Reductions in air conditioning energy caused by a nearby park. *Energy and Buildings*, *29*(1), 83-92

Cao, X., Onishi, A., Chen, J., & Imura, H. (2010). Quantifying the cool island intensity of urban parks using ASTER and IKONOS data. *Landscape and Urban Planning*, *96*(4), 224-231.

Carrasco-Hernandez, R., Smedley, A. R. D., & Webb, A. R. (2015). Using urban canyon geometries obtained from Google Street View for atmospheric studies: Potential applications in the calculation of street level total shortwave irradiances. *Energy and Buildings*, *86*, 340–348.

Chang, C. R., Li, M. H., & Chang, S. D. (2007). A preliminary study on the local cool-island intensity of Taipei city parks. *Landscape and Urban Planning*, *80*(4), 386-395.

Charlton, M., Fotheringham, S., & Brunsdon, C. (2009). Geographically weighted regression. *White paper. National Centre for Geocomputation. National University of Ireland Maynooth*.

Cheng, X., Wei, B., Chen, G., Li, J., & Song, C. (2014). Influence of park size and its surrounding urban landscape patterns on the park cooling effect. *Journal of Urban Planning and Development*, *141*(3), A4014002.

Church, R. L., & Murray, A. T. (2009). *Business site selection, location analysis, and GIS*. Hoboken, NJ: John Wiley & Sons.

Church, R. L., & ReVelle, C. (1974). The maximal covering location problem. *Papers in Regional Science*, *32*(1), 101-118.

Chow, W. T., Pope, R. L., Martin, C. A., & Brazel, A. J. (2011). Observing and modeling the nocturnal park cool island of an arid city: horizontal and vertical impacts. *Theoretical and Applied Climatology*, *103*(1-2), 197-211.

Chow, W. T. L., & Brazel, A. J. (2012). Assessing xeriscaping as a sustainable heat island mitigation approach for a desert city. *Building and Environment*, *47*(1), 170–181.

Chuang, W. C., & Gober, P. (2015). Predicting hospitalization for heat-related illness at the census-tract level: Accuracy of a generic heat vulnerability index in phoenix, Arizona (USA). *Environmental health perspectives*, *123*(6), 606.

City of Phoenix, 2008. Downtown Phoenix Urban Form Project, Available at: http://phoenix.gov/pdd/pz/dtplan.html

City of Phoenix, 2010. Tree and Shade Master Plan, Available at: http://phoenix.gov/webcms/groups/internet/@inter/@dept/@parks/documents/web content

Coseo, P., & Larsen, L. (2014). How factors of land-use/land-cover, building configuration, and adjacent heat sources and sinks explain Urban Heat Islands in Chicago. *Landscape and Urban Planning*, *125*, 117-129.

Czarnota, J., Wheeler, D. C., & Gennings, C. (2015). Evaluating geographically weighted regression models for environmental chemical risk analysis. *Cancer informatics*, *14*, CIN-S17296.

Da Silva, A. R., & Fotheringham, A. S. (2016). The multiple testing issue in geographically weighted regression. *Geographical Analysis*, *48*(3), 233-247.

Dale, M. R. T., & Fortin, M. J. (2002). Spatial autocorrelation and statistical tests in ecology. *Ecoscience*, *9*(2), 162–167.

Eliasson, I., & Upmanis, H. (2000). Nocturnal airflow from urban parks-implications for city ventilation. *Theoretical and Applied Climatology*, *66*(1-2), 95-107.

Erell, E., Pearlmutter, D., & Williamson, T. (2012). Urban microclimate: designing the spaces between buildings. *Routledge*.

Fan, C., Myint, S. W., & Zheng, B. (2015). Measuring the spatial arrangement of urban vegetation and its impacts on seasonal surface temperatures. *Progress in Physical Geography*, *39*(2), 199-219.

Fan, C., Rey, S. J., & Myint, S. W. (2017). Spatially filtered ridge regression (SFRR): A regression framework to understanding impacts of land-cover patterns on urban climate. *Transactions in GIS*, *21*(5), 862-879.

Fan, H., & Sailor, D. J. (2005). Modeling the impacts of anthropogenic heating on the urban climate of Philadelphia: a comparison of implementations in two PBL schemes. *Atmospheric Environment*, *39*(1), 73-84.

Fernández, F. J., Alvarez-Vázquez, L. J., García-Chan, N., Martínez, A., & Vázquez-Méndez, M. E. (2015). Optimal location of green zones in metropolitan areas to control the urban heat island. *Journal of Computational and Applied Mathematics*, *289*, 412-425.

Flaxman, M. (2010). Fundamentals of geodesign. *Proceedings of Digital Landscape Architecture, Anhalt University of Applied Science*, *2*, 28-41.

Forman, R. T. T. (2016). Urban ecology principles: are urban ecology and natural area ecology really different? *Landscape Ecology*, 1–10.

Fotheringham, A. S., Brunsdon, C., & Charlton, M. (2002). *Geographically Weighted Regression: The Analysis of Spatially Varying Relationships*. Wiley.

Fung, W. Y., Lam, K. S., Hung, W. T., Pang, S. W., & Lee, Y. L. (2006). Impact of urban temperature on energy consumption of Hong Kong. *Energy*, *31*(14), 2623-2637.

Fung, W. Y., Lam, K. S., Nichol, J., & Wong, M. S. (2009). Derivation of nighttime urban air temperatures using a satellite thermal image. *Journal of Applied Meteorology and Climatology*, *48*(4), 863-872.

Georgescu, M., Morefield, P. E., Bierwagen, B. G., & Weaver, C. P. (2014). Urban adaptation can roll back warming of emerging megapolitan regions. *Proceedings of the National Academy of Sciences*, *111*(8), 2909-2914.

Gillespie, A. R., Rokugawa, S., Hook, S. J., Matsunaga, T., & Kahle, A. B. (1999). Temperature/emissivity separation algorithm theoretical basis document, version 2.4. *ATBD contract NAS5-31372, NASA*.

Gober, P., Brazel, A., Quay, R., Myint, S., Grossman-Clarke, S., Miller, A., & Rossi, S. (2009). Using watered landscapes to manipulate urban heat island effects: how much water will it take to cool Phoenix?. *Journal of the American Planning Association*, *76*(1), 109-121.

Grimm, N. B., Faeth, S. H., Golubiewski, N. E., Redman, C. L., Wu, J., Bai, X., … Briggs, J. M. (2015). Global Change and the Ecology of Cities. *Science*, *319*(5864), 756–760.

Grimmond, C. S. B., & Oke, T. R. (2002). Turbulent heat fluxes in urban areas: observations and a local-scale urban meteorological parameterization scheme (LUMPS). *Journal of Applied Meteorology*, *41*(7), 792-810.

Harlan, S. L., Brazel, A. J., Prashad, L., Stefanov, W. L., & Larsen, L. (2006). Neighborhood microclimates and vulnerability to heat stress. *Social Science & Medicine*, *63*(11), 2847-2863.

Hartz, D. A., Prashad, L., Hedquist, B. C., Golden, J., & Brazel, A. J. (2006). Linking satellite images and hand-held infrared thermography to observed neighborhood climate conditions. *Remote Sensing of Environment*, *104*(2), 190-200.

Hondula, D. M., Davis, R. E., Leisten, M. J., Saha, M. V., Veazey, L. M., & Wegner, C. R. (2012). Fine-scale spatial variability of heat-related mortality in Philadelphia

County, USA, from 1983-2008: a case-series analysis. *Environmental Health*, *11*(1), 1.

Hondula, D. M., Vanos, J. K., & Gosling, S. N. (2014). The SSC: a decade of climate–health research and future directions. *International Journal of Biometeorology*, *58*(2), 109-120.

Hu, T., Liu, Q., Du, Y., Li, H., Wang, H., & Cao, B. (2015). Analysis of the land surface temperature scaling problem: A case study of airborne and satellite data over the Heihe Basin. *Remote Sensing*, *7*(5), 6489-6509.

Huang, G., Zhou, W., & Cadenasso, M. L. (2011). Is everyone hot in the city? Spatial pattern of land surface temperatures, land-cover and neighborhood socioeconomic characteristics in Baltimore, MD. *Journal of Environmental Management*, *92*(7), 1753-1759.

Hulley, G. C., Hughes, C. G., & Hook, S. J. (2012). Quantifying uncertainties in land surface temperature and emissivity retrievals from ASTER and MODIS thermal infrared data. *Journal of Geophysical Research: Atmospheres*, *117*(D23).

Hurvich, C. M., Simonoff, J. S., & Tsai, C. L. (1998). Smoothing parameter selection in nonparametric regression using an improved Akaike information criterion. *Journal of the Royal Statistical Society: Series B (Statistical Methodology)*, *60*(2), 271-293.

Imhoff, M. L., Zhang, P., Wolfe, R. E., & Bounoua, L. (2010). Remote sensing of the urban heat island effect across biomes in the continental USA. *Remote sensing of environment*, *114*(3), 504-513.

Jenerette, G. D., Harlan, S. L., Stefanov, W. L., & Martin, C. A. (2011). Ecosystem services and urban heat riskscape moderation: water, green spaces, and social inequality in Phoenix, USA. *Ecological Applications*,*21*(7), 2637-2651.

JPL. (2001). ASTER Higher-Level Product User Guide, Advanced Spaceborne Thermal Emission and Reflection Radiometer. *Jet Propulsion Laboratory*, California Institute of Technology.

Jusuf, S. K., Wong, N. H., Tan, C. L., & Tan, A. Y. K. (2012). STEVE tool: Bridging the gap between urban climatology research and urban planning process. *In ICSDC 2011: Integrating Sustainability Practices in the Construction Industry* (pp. 25-33).

Kamarianakis, Y., Li, X., Turner, B. L., & Brazel, A. J. (2017). On the effects of landscape configuration on summer diurnal temperatures in urban residential areas: application in Phoenix, AZ. *Frontiers of Earth Science*, 1–19.

Klok, L., Zwart, S., Verhagen, H., & Mauri, E. (2012). The surface heat island of Rotterdam and its relationship with urban surface characteristics. *Resources, Conservation and Recycling*, *64*, 23-29.

Kottek, M., Grieser, J., Beck, C., Rudolf, B., & Rubel, F. (2006). World map of the Köppen-Geiger climate classification updated. *Meteorologische Zeitschrift*, *15*(3), 259-263.

Krayenhoff, E. S., & Voogt, J. A. (2016). Daytime thermal anisotropy of urban neighbourhoods: Morphological causation. *Remote Sensing*, *8*(2), 108.

Legendre, P., & Fortin, M. J. (1989). Spatial pattern and ecological analysis. *Vegetatio*, *80*(2), 107–138.

Li, X., Li, W., Middel, A., Harlan, S. L., Brazel, A. J., & Turner, B. L. (2016). Remote sensing of the surface urban heat island and land architecture in Phoenix, Arizona: Combined effects of land composition and configuration and cadastral–demographic–economic factors. *Remote Sensing of Environment*, *174*, 233-243.

Li, X., Myint, S. W., Zhang, Y., Galletti, C., Zhang, X., & Turner, B. L. (2014). Object-based land-cover classification for metropolitan Phoenix, Arizona, using aerial photography. *International Journal of Applied Earth Observation and Geoinformation*, *33*, 321-330.

Li, X., Ratti, C., & Seiferling, I. (2018). Quantifying the shade provision of street trees in urban landscape: A case study in Boston, USA, using Google Street View. *Landscape and Urban Planning*, *169*, 81-91.

Li, X., Zhou, W., & Ouyang, Z. (2013). Relationship between land surface temperature and spatial pattern of greenspace: What are the effects of spatial resolution? *Landscape and Urban Planning*, *114*, 1–8.

Li, W., Goodchild, M. F., & Church, R. (2013). An efficient measure of compactness for two-dimensional shapes and its application in regionalization problems. *International Journal of Geographical Information Science*, *27*(6), 1227-1250.

Lin, W., Yu, T., Chang, X., Wu, W., & Zhang, Y. (2015). Calculating cooling extents of green parks using remote sensing: Method and test. *Landscape and Urban Planning*, *134*, 66-75.

Liu, W., Feddema, J., Hu, L., Zung, A., & Brunsell, N. (2017). Seasonal and diurnal characteristics of land surface temperature and major explanatory factors in Harris County, Texas. *Sustainability*, *9*(12), 2324.

Long, J., Shelhamer, E., & Darrell, T. (2015). Fully convolutional networks for semantic segmentation. In *Proceedings of the IEEE conference on computer vision and pattern recognition* (pp. 3431-3440).

Lukasczyk, J., Middel, A., Zakrzewski, S., Arnold, M., Maciejewski, R. (nd.) Urban Form and Composition of Street Canyons: A Human-Centric Big Data and Deep Learning Approach. *Landscape and Urban Planning* (under review).

McGarigal, K., & Marks, B. J. (1995). Spatial pattern analysis program for quantifying landscape structure. Gen. Tech. Rep. PNW-GTR-351. *US Department of Agriculture, Forest Service, Pacific Northwest Research Station*.

Meier, A., & Taha, H. (2000). Mitigation of urban heat islands: meteorology, energy, and air quality impact. *Journal of Architecture, Planning and Environmental Engineering*, *529*: 69-76.

Middel, A., Häb, K., Brazel, A. J., Martin, C. A., & Guhathakurta, S. (2014). Impact of urban form and design on mid-afternoon microclimate in Phoenix Local Climate Zones. *Landscape and Urban Planning, 122*, 16-28.

Middel, A., Chhetri, N., & Quay, R. (2015). Urban forestry and cool roofs: Assessment of heat mitigation strategies in Phoenix residential neighborhoods. *Urban Forestry and Urban Greening, 14*(1), 178–186.

Middel, A., Lukasczyk, J., & Maciejewski, R. (2017). Sky view factors from synthetic fisheye photos for thermal comfort routing—a case study in Phoenix, Arizona. *Urban Planning*, *2*(1), 19.

Murray, A. T. (2010). Advances in location modeling: GIS linkages and contributions. *Journal of Geographical Systems*, *12*(3), 335–354.

Murray, A. T., Tong, D., & Kim, K. (2010). Enhancing classic coverage location models. *International Regional Science Review, 33*(2), 115-133.

Myint, S. W., Wentz, E. A., Brazel, A. J., & Quattrochi, D. A. (2013). The impact of distinct anthropogenic and vegetation features on urban warming. *Landscape ecology*, *28*(5), 959-978.

Myint, S. W., Zheng, B., Talen, E., Fan, C., Kaplan, S., Middel, A., Smith., M,Huang, H & Brazel, A. (2015). Does the spatial arrangement of urban landscape matter? Examples of urban warming and cooling in Phoenix and Las Vegas. *Ecosystem Health and Sustainability*, *1*(4), 1-15.

Neema, M. N., & Ohgai, A. (2013). Multitype green-space modeling for urban planning using GA and GIS. *Environment and Planning B: Planning and Design*, *40*(3), 447-473.

Ng, E., Chen, L., Wang, Y., & Yuan, C. (2012). A study on the cooling effects of greening in a high-density city: an experience from Hong Kong. *Building and Environment*, *47*, 256-271.

Nichol, J. E., Fung, W. Y., Lam, K. S., & Wong, M. S. (2009). Urban heat island diagnosis using ASTER satellite images and 'in situ'air temperature. *Atmospheric Research*, *94*(2), 276-284.

Oke, T. R. (1988). The urban energy balance. *Progress in Physical geography*, *12*(4), 471-508.

Polsky, C., Grove, J. M., Knudson, C., Groffman, P. M., Bettez, N., Cavender-Bares, J. & Morse, J. L. (2014). Assessing the homogenization of urban land management with an application to US residential lawn care. *Proceedings of the National Academy of Sciences*, *111*(12), 4432-4437.

Ren, Z., He, X., Zheng, H., Zhang, D., Yu, X., Shen, G., & Guo, R. (2013). Estimation of the relationship between urban park characteristics and park cool island intensity by remote sensing data and field measurement. *Forests*, *4*(4), 868-886.

Richards, D. R., & Edwards, P. J. (2017). Quantifying street tree regulating ecosystem services using Google Street View. *Ecological Indicators*, *77*, 31-40.

Ruddell, D. M., Harlan, S. L., Grossman-Clarke, S., & Buyantuyev, A. (2010). Risk and exposure to extreme heat in microclimates of Phoenix, AZ. In *Geospatial techniques in urban hazard and disaster analysis* (pp. 179-202). Springer Netherlands.

Ruddell, D., Hoffman, D., Ahmad, O., & Brazel, A. (2013). Historical threshold temperatures for Phoenix (urban) and Gila Bend (desert), central Arizona, USA. *Climate Research*, *55*(3), 201-215.

Sailor, D. J. (2001). Relating residential and commercial sector electricity loads to climate-evaluating state level sensitivities and vulnerabilities. *Energy*, *26*(7), 645-657.

Seto, K. C., & Reenberg, A. (Eds.). (2014). *Rethinking global land-use in an urban era* (Vol. 14). MIT Press.

Seto, K. C., Golden, J. S., Alberti, M., & Turner, B. L. (2017). Sustainability in an urbanizing planet. *Proceedings of the National Academy of Sciences, 114*(34), 8935-8938.

Shashua-Bar, L., Pearlmutter, D., & Erell, E. (2009). The cooling efficiency of urban landscape strategies in a hot dry climate. *Landscape and Urban Planning, 92*(3), 179-186.

Song, J., Wang, Z. H., Myint, S. W., & Wang, C. (2017). The hysteresis effect on surface-air temperature relationship and its implications to urban planning: An examination in Phoenix, Arizona, USA. *Landscape and Urban Planning, 167*, 198-211.

Spronken-Smith, R. A., & Oke, T. R. (1998). The thermal regime of urban parks in two cities with different summer climates. *International Journal of Remote Sensing*, *19*(11), 2085-2104.

Spronken-Smith, R. A., & Oke, T. R. (1999). Scale modelling of nocturnal cooling in urban parks. *Boundary-Layer Meteorology*, *93*(2), 287-312.

Spronken-Smith, R. A., Oke, T. R., & Lowry, W. P. (2000). Advection and the surface energy balance across an irrigated urban park. *International Journal of Climatology*, *20*(9), 1033-1047.

Stewart, I. D., & Oke, T. R. (2012). Local climate zones for urban temperature studies. *Bulletin of the American Meteorological Society*, *93*(12), 1879–1900.

Stewart, I. D., Oke, T. R., & Krayenhoff, E. S. (2014). Evaluation of the 'local climate zone'scheme using temperature observations and model simulations. *International Journal of Climatology*, *34*(4), 1062-1080.

Stoll, M. J., & Brazel, A. J. (1992). Surface-air temperature relationships in the urban environment of Phoenix, Arizona. *Physical Geography*, *13*(2), 160-179.

Tobler, W. R. (1970). A computer movie simulating urban growth in the Detroit region. *Economic geography*, *46*(sup1), 234-240.

Turner II, B. L. (2017). Land system architecture for urban sustainability: new directions for land system science illustrated by application to the urban heat island problem. *Journal of Land-use Science*, *12*(6), 689–697.

Unger, J. (2004). Intra-urban relationship between surface geometry and urban heat island: review and new approach. *Climate Research*, *27*, 253–264.

Unger, J. (2008). Connection between urban heat island and sky view factor approximated by a software tool on a 3D urban database. *International Journal of Environment and Pollution*, *36*(1-3), 59-80.

Upmanis, H., Eliasson, I., & Lindqvist, S. (1998). The influence of green areas on nocturnal temperatures in a high latitude city (Göteborg, Sweden).*International Journal of Climatology*, *18*(6), 681-700.

Voogt, J. A., & Oke, T. R. (2003). Thermal remote sensing of urban climates. *Remote Sensing of Environment*, *86*(3), 370-384.

Wang, C., Middel, A., Myint, S. W., Kaplan, S., Brazel, A. J., & Lukasczyk, J. (2018). Assessing local climate zones in arid cities : The case of Phoenix, Arizona and Las Vegas, Nevada. *ISPRS Journal of Photogrammetry and Remote Sensing*, *141*, 59–71.

Weng, Q. (2009). Thermal infrared remote sensing for urban climate and environmental studies: Methods, applications, and trends. *ISPRS Journal of Photogrammetry and Remote Sensing*, *64*(4), 335-344.

Wentz, E. A., Rode, S., Li, X., Tellman, E. M., & Turner, B. L. (2016). Impact of Homeowner Association (HOA) landscaping guidelines on residential water use. *Water Resources Research*, *52*(5), 3373-3386.

Wheeler, D., & Tiefelsdorf, M. (2005). Multicollinearity and correlation among local regression coefficients in geographically weighted regression. *Journal of Geographical Systems*, *7*(2), 161-187.

Wheeler, M. M., Neill, C., Groffman, P. M., Avolio, M., Bettez, N., Cavender-Bares, J., Chowdhury, R.R., Darling, L., Grove, J.M., Hall, S.J. & Heffernan, J. B. (2017). Continental-scale homogenization of residential lawn plant communities. *Landscape and Urban Planning*, *165*, 54-63.

Wong, N. H., Jusuf, S. K., & Tan, C. L. (2011). Integrated urban microclimate assessment method as a sustainable urban development and urban design tool. *Landscape and Urban Planning*, *100*(4), 386-389.

Wu, J. (2013). Landscape sustainability science: ecosystem services and human well-being in changing landscapes. *Landscape Ecology*, *28*(6), 999-1023.

Yamaguchi, Y., Kahle, A. B., Tsu, H., Kawakami, T., & Pniel, M. (1998). Overview of advanced spaceborne thermal emission and reflection radiometer (ASTER). *IEEE Transactions on geoscience and remote sensing*, *36*(4), 1062-1071.

Yu, Z., Xu, S., Zhang, Y., Jørgensen, G., & Vejre, H. (2018). Strong contributions of local background climate to the cooling effect of urban green vegetation. *Scientific reports, 8*(1), 6798.

Yu, Z., Guo, X., Zeng, Y., Koga, M., & Vejre, H. (2018). Variations in land surface temperature and cooling efficiency of green space in rapid urbanization: The case of Fuzhou city, China. *Urban Forestry & Urban Greening, 29*, 113-121.

Zhao, Q., Sailor, D. J., & Wentz, E. A. (2018). Impact of tree locations and arrangements on outdoor microclimates and human thermal comfort in an urban residential environment. *Urban Forestry & Urban Greening, 32*, 81-91.

Zhang, Y., Murray, A. T., & Turner, B. L. (2017). Optimizing green space locations to reduce daytime and nighttime urban heat island effects in Phoenix, Arizona. *Landscape and Urban Planning, 165*, 162-171.

Zhang, W., & Huang, B. (2014). Land-use optimization for a rapidly urbanizing city with regard to local climate change: Shenzhen as a case study. *Journal of Urban Planning and Development, 141*(1), 05014007.

Zhou, W., Huang, G., & Cadenasso, M. L. (2011). Does spatial configuration matter? Understanding the effects of land-cover pattern on land surface temperature in urban landscapes. *Landscape and Urban Planning, 102*(1), 54–63.